paesaggio
diverso

Gletschersee und Wasserkraft.

Sedimentation eines Gletschersees.
ETH Semesterarbeit, G. Odermatt
Supervisor: Prof. Dr. Daniel Farinotti and Prof. Dr. Nathalie Dubois
Mentor: Ronald Lloren,
Laboratory of Hydraulics, Hydrology and Glaciology (VAW)
Swiss Federal Insitute of Aquatic Science and Technology (Eawag)
ETH Zürich

Die Sedimentation des Stausees bleibt ein kritischer Faktor, wenn die Stauung eines Gletschersees zur Wasserkraftnutzung in Betracht gezogen wird.

paesaggiodiverso - planungsbüro für landschaft und gewässer
steinberggasse 2 - 8400 winterthur - telefon 052 212 19 35 - https://www.paesaggiodiverso.ch

Vergleich der Sedimentdynamik eines natürlichen und eines aufgestauten Gletschersees.

Dieses Semesterprojekt ist Teil des TapRep-Projekts im Rahmen des Arbeitspakets 3 mit dem Titel «Quantifying periglacial sediment dynamics at the multi- catchment scale». Das Projekt ist eine Zusammenarbeit zwischen der Versuchsanstalt für Wasserbau, Hydrologie und Glaziologie (VAW) der Eidgenössischen Technischen Hochschule Zürich (ETH), der Universität Zürich (UZH), der Eidgenössischen Anstalt für Wasserversorgung, Abwasserreinigung und Gewässerschutz (Eawag) und der Universität Lausanne (UNIL). Der Schwerpunkt dieses Semesterprojekts lag auf der Untersuchung von zwei Gletscherseen, um ein besseres Verständnis der Verlandung in diesen Umgebungen zu erlangen.

Die Studienorte waren der Triftsee im Kanton Bern, ein natürlicher und noch unberührter Gletschersee, und der Griessee, ein gestauter Gletschersee. Für jeden See wurde ein Sedimentkern entnommen und im Labor von Eawag in Dübendorf mit verschiedenen Methoden analysiert: Zeilenscan für hochauflösende Bilder, XRF-Analyse zur Bestimmung der Elementzusammensetzung, Korngrössenanalyse für Ton-, Schluff- und Sandfraktionen, Messung der Trockenschüttdichte und des Wassergehalts, Berechnung der Massenakkumulationsrate und Gammaspektroskopie (basierend auf ^{10}Pb, ^{137}Cs, and ^{7}Be isotopes) zur Datierung.

Die Ergebnisse zeigten eine visuell deutliche Schichtung im Kern des Triftsees, während diese im Griessee nicht sichtbar war. In beiden Seen dominierte der Schluffanteil, wobei der Triftsee einen höheren Tonanteil aufwies, während der Griessee einen höheren Sandanteil hatte. Die Elementzusammensetzung lieferte interessante Erkenntnisse über Signale aus dem Einzugsgebiet, wie z.B. einen höheren Sedimenteintrag, der durch erhöhte Al/Ti- und Si/Ti-Werte gekennzeichnet ist. Die Gamma-Analyse ergab für den Triftsee eine Sedimentationsrate von etwa 0,91 cm/a, während die Gamma-Analyse des Griessees keine eindeutigen Ergebnisse lieferte. Zusätzliche Untersuchungen, die auf bathymetrischen Messungen der letzten Jahrzehnte sowie auf Korngrößenanalysen und Signalen der Elementzusammensetzung basierten, ergaben für den Griessee eine Sedimentationsrate von etwa 2-3 cm/a. Die Unterschiede in der Sedimentation wurden auf verschiedene Merkmale des Einzugsgebiets zurückgeführt, darunter Niederschlag, Gletscherrückgang, Geologie und Gefälle, aber auch auf die Tatsache, dass der Griessee aufgestaut ist. Daraus lässt sich schließen, dass die Sedimentation des Stausees ein kritischer Faktor bleibt, wenn die Stauung eines Gletschersees zur Wasserkraftnutzung in Betracht gezogen wird.

paesaggio
diverso

Gletschersee und Wasserkraft.
Sedimentation eines Gletschersees.

paesaggiodiverso - planungsbüro für landschaft und gewässer
steinberggasse 2 - 8400 winterthur - telefon 052 212 19 35 - https://www.paesaggiodiverso.ch

ETH
Eidgenössische Technische Hochschule Zürich
Swiss Federal Institute of Technology Zurich

Comparing the sediment dynamics of a natural and a dammed glacier lake

Semester Project

Georg Odermatt

December 22, 2023

Supervisor: Prof. Dr. Daniel Farinotti and Prof. Dr. Nathalie Dubois
Mentor: Ronald Lloren

Laboratory of Hydraulics, Hydrology and Glaciology (VAW)
Swiss Federal Insitute of Aquatic Science and Technology (Eawag)
ETH Zürich

Contents

Chapter 1

Introduction

1.1 Motivation

Climate change is impacting ice sheets and glaciers worldwide (Vuille et al., 2008). These large accumulations of ice are good indicators reflecting the negative impacts of climate change, especially the warming trend (Hock & Huss, 2021). The melting of ice sheets, especially at the poles, leads to hydrological changes and a rising sea level (Chen et al., 2013). Similar processes are happening with alpine glaciers, resulting in a range of consequences, from modified natural hazards to alterations in the hydrological patterns of these areas. Glaciers play a dual role in geomorphological processes (Aber, 2008). On one hand, they contribute significantly to the erosion of materials as they melt (Ballantyne, 2002). On the other hand, they serve as agents of transport, conveying eroded materials and sediments that subsequently deposit in downstream lakes (Ballantyne, 2002). The alteration of the hydrological patterns and the deposition of sediments have significant implications for hydropower production (Huss, 2011). Therefore, it is crucial to monitor glacier changes to gain a deeper understanding of the interlinked mechanisms of melting and erosion processes, enable future forecasting, and take suitable measures (Haeberli et al., 2007).

Switzerland, with its vast mountainous terrain and the majestic Alps, is home to a multitude of glaciers and glacier lakes, owing to its unique geography and topography (Salim, 2022). As glaciers continue to melt, numerous lakes will be formed in the alpine region (Steffen et al., 2022). These lakes serve as vital ecosystems for alpine flora and fauna, while also playing a crucial role in the water balance of their respective catchment areas. Some of these lakes have already been dammed and are used for water storage and hydropower generation. With the Swiss Energy Strategy 2050, calling for an expansion of hydropower capacity, there is a significant interest in the potential of the recently created lakes. These bodies of water present

an opportunity not only for enhanced energy production but also for the efficient storage and redistribution of solar photovoltaic-generated power, facilitating a transition from summer to winter energy demands. However, it is unclear how long these lakes will exist, as on the one hand, the glaciers will eventually completely melt leading to a decrease in water input from the catchment, and on the other hand, the glacier lakes will be filled with transported material from the glacier. The use of glacier lakes is a politically sensitive issue because the interests of the use of renewable energies conflict with the interests of environmental and landscape protection.

Sedimentation means the deposition in a lake of material eroded in the catchment (Callieri, 1997). It is a key parameter for the longevity and sustainability of reservoirs (Wisser et al., 2013) and a growing worldwide issue that is anticipated to worsen in the near future due to climate change, resulting in a greater supply of sediment from receding glaciers (Ehrbar et al., 2018). Consequently, there is a rising demand for effective sediment management to preserve the operational water storage capacity in reservoirs and ensure the uninterrupted flow of sediment along rivers, from upstream to downstream of dam structures (Schleiss et al., 2016). Globally, the current trend indicates a decline in net storage as the rate of sedimentation outpaces the installation of new storage facilities (Wisser et al., 2013). The removal of deposited sediments in reservoires necessitates annual investments ranging from 13 to 19 trillion US dollars on a global scale (Schleiss et al., 2016).

This semester-project is embedded in the TapRep project (tapping the potential of one decade of annual repeat altimetry to study glacial and periglacial processes), which aims to leverage the unique «Spezialbefliegungen» dataset, consisting of high-resolution aerial photographs and digital elevation models, to advance the understanding of glaciological processes in the Swiss Alps. The TapRep project focuses on improving the extrapolation of glacier mass balance, assessing surface-collapse features on glacier tongues, and quantifying periglacial sediment dynamics. Additionally, 3D visualizations of the annual data will be created for effective public outreach. This semester project relates to the working package 3 «Quantifying periglacial sediment dynamics at the multi-catchment scale».

This semester project will evaluate recent sedimentation in two glacier lakes from the Swiss Alps. This should help to better understand sedimentation processes in glacier lakes, especially regarding the usage of glacier lakes as reservoirs for hydropower production.

1.2 Background and State of Research

Considering the spatiotemporal dynamics of sedimentation in newly formed glacier lakes is crucial, as many overdeepenings are likely to be filled with sediment within a few years of their formation (Mölg et al., 2021). A study conducted by Steffen et al. (2022) marks the first attempt to assess the potential impact of sedimentation on the formation of new glacier lakes in bedrock overdeepenings. The assessment states the importance of sedimentation, especially in the early stages of small proglacial lakes. The model employed in the study suggests that, for the broader region of the Alps and depending on the climate scenario, 11% to 32% of the potential new lake volume may be filled with sediments by 2100. While factors such as the actual volume of overdeepenings and their potential water fill-up remain critical, the findings emphasize that sediment input systematically reduces future glacier lake volumes, also stated by (Swift et al., 2021). The study by Steffen et al. (2022) stresses that neglecting this effect would lead to an overestimate of potential future glacier lake volumes, aligning with the findings in (Cook & Swift, 2012). It also emphasizes the need to enhance understanding of related processes, especially given the observed increase in sediment.

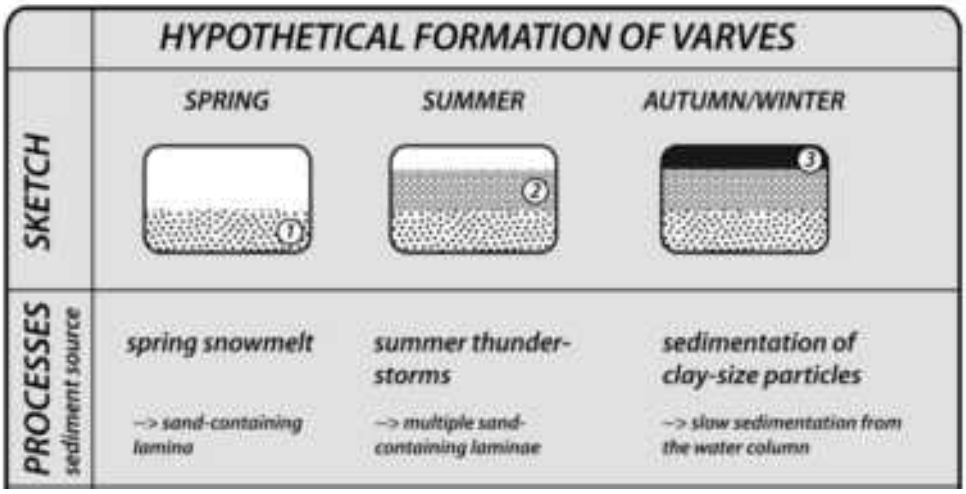

Figure 1.1: Hypothetical varve formation (Mauchle, 2010).

In glacierized catchments, erosion processes are directly linked to the dynamics of glaciers (Delaney et al., 2017). As glaciers melt, they contribute to the erosion of surrounding materials, starting a cascade of sediment transport downstream (Menzies & Ross, 2020). The annual deposition of sediments may result in distinct layers and lamination (Leonard, 1986). Throughout the year, consistent processes, driven by glacier melting, lead to the formation of this lamination. Contrasting layers of sediment are deposited in

the melting and the non-melting seasons (Zolitschka et al., 2015). This lamination ideally reflects annual varves, enabling the dating of sediment at various depths, similar to the way tree varves are utilized. Identifying these varves can help to better understand sedimentation processes in glacier lakes and reservoirs (Zolitschka et al., 2015). Dense meltwater with high sediment concentration results in the deposition of silty to sandy layers, whereas winter deposition is marked by clay beds due to the freezing of the lake surface (Zolitschka et al., 2015). When analyzing the signals in the varves, it is important to distinguish between "continuous records" from "event-records" (Arnaud et al., 2016). A study by Mauchle (2010) observed significant variations in particle flux, grain size distributions, and mineral composition over an annual cycle of sedimentation for a glacier lake in the Swiss Alps. The study came up with a visual representation of the hypothetical properties of an individual varve (Figure 1.1).

1.3 Research Objectives

In this semester project, we would like to understand:

1. What are the differences in sedimentation of a natural and a dammed glacier lake?

2. What is the speed at which sedimentation is occurring (sedimentation rate)?

The overall objective of this study is to determine the duration it takes for a natural glacier lake and a dammed glacier lake to accumulate sediments. To achieve this, the sedimentation of both lakes will be thoroughly investigated and compared. By analyzing sediment cores from the lakes, the overall sedimentation rate of the glacier lakes will be estimated. These findings could serve to better understand the sedimentation process in glacier lakes and probably help for assessing the economic viability of utilizing glacier lakes as a storage reservoir for hydropower. Furthermore, the sedimentation rates can be compared with the glacier melting process and terrain change of the «Spezialbefliegungen» pictures.

Chapter 2

Study Sites

Five lakes were selected as potential sites of investigation for the sedimentation part of the TapRep project. These are:

- Oberaarsee (BE)
- Griessee (VS)
- Small lake in front of Silvrettagletscher (GR)
- Turtmann (VS)
- Triftsee (BE)

Figure 2.1: Picture of Triftsee taken during the fieldwork on board the Swiss military helicopter (Credits: Georg Odermatt).

For this semester project, the focus was on two of these lakes: 1) Lake Griess (hereinafter referred to Griessee) in the canton of Valais below the Gries glacier, and 2) Lake Trift (hereinafter referred to Triftsee), below the Trift glacier. These lakes were chosen because of their similar sizes, making the results more comparable. Furthermore, Griessee is an artificial lake

with a built-dam infrastructure, which is used as a storage reservoir for hydropower (Figure 2.2), while Triftsee is a natural and as yet unused lake (Figure 2.1), but there are plans to also dam the Triftsee. This allows us to investigate the impact of dam and lake usage for hydropower on sediment dynamics.

In the following sections, the foundational aspects of the study sites are examined. Firstly, the dynamics of the glaciers feeding the lakes are explored. Secondly, the geological characteristics in the surrounding of the lakes are investigated. Last but not least, the hydrology of the watershed is analyzed. The geological context is of significance as it enables the identification of the types of materials introduced into the lake through (glacier-) erosion processes and subsequently deposited as sediment (Arnaud et al., 2016). This, in turn, may potentially be linked to the glacier retreat and the sedimentation process within the lake. The hydrology within the watershed plays a role in the sense that it impacts the glacier's dynamics and, indirectly, the erosion and material transport processes triggered by glacier retreat, as well as the overall water dynamics within the lake (Huss et al., 2010).

Figure 2.2: Picture of Griessee showing the dam structure and the glacier (Wikipedia, 2008).

2.1 Trift

Until 1973, the glacier extended to the location where the lake is currently situated (Figure A.1 in Appendix). It wasn't until the beginning of this millennium that Triftsee came into existence (Figure A.3 in Appendix). What makes this lake particularly unique is that its formation was facilitated by a geological feature known as a «Riegel» (Steinemann et al., 2021). This «Riegel» spans approximately 0.9 kilometers in width and extends 1.5 kilometers in length. The dynamic force of the water has sculpted an overdeepening between the glacier and the «Riegel», creating space for the water to accumulate and form a lake. The lake is situated at an elevation of 1650 meters above sea level (m.a.s.l.). It covers an area of approximately 0.2 km^2 (length of around 700 meters and width of around 300 meters) and attains maximal depths of approximately 60 meters, which strongly vary depending on the inflow of meltwater over the year.

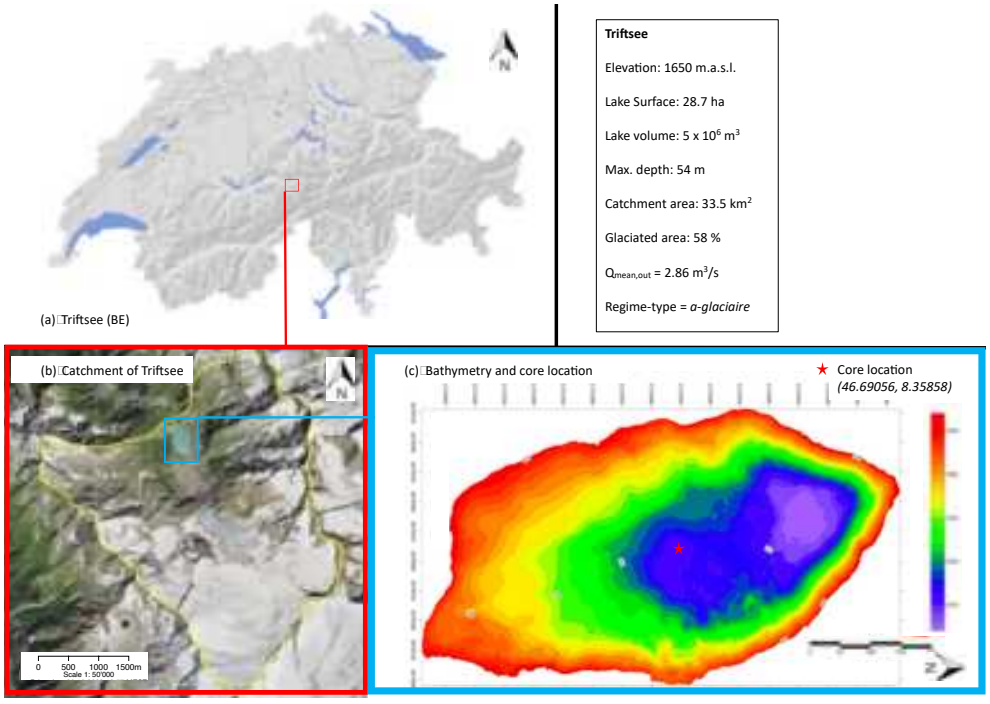

Figure 2.3: Location of Triftsee on the topographical map of Switzerland together with catchment on aerial photograph and lake bathymetry. Bathymetry of Triftsee was measured in 2023 by RBR Geophysics.

The bathymetry of the lake is depicted in Figure 2.3 together with the location of the lake and the catchment on an aerial image.
Geophysical data suggest a lacustrine sediment thickness in the range of 2 to 6 meters (Grischott et al., 2010). The lake's water level, maintained at

an elevation of 1650 m.a.s.l., is regulated by a deep gorge of approximately 100 meters in depth that intersects the transverse moraine (Steinemann et al., 2021). The formation of the lake in front of the Trift glacier was closely monitored due to the potential hazard of a sudden glacier tongue collapse and subsequent glacial outburst flood, as documented in studies by Dalban Canassy et al. (2011).

2.1.1 Glacier

The current thickness of the glacier averages around 50 meters, with values up to 500 meters (Figure A.4). In Figure 2.4, the ice volume and the area of the Trift Glacier for the past nearly hundred years are depicted. The data were provided by the Laboratory of Hydraulics, Hydrology and Glaciology (VAW) of ETH Zurich. This graph illustrates that both the volume and the area decrease relatively uniformly. Since the 1980s, this decrease has intensified.

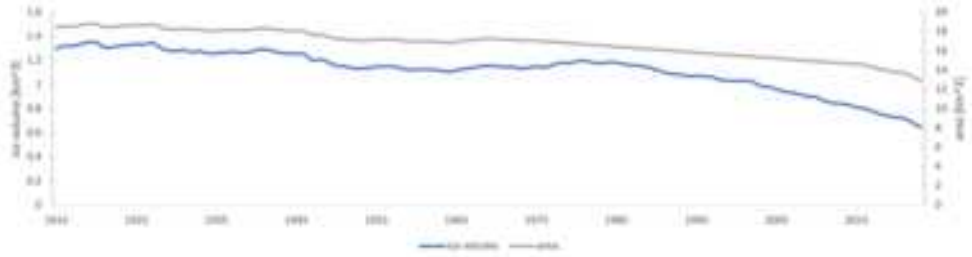

Figure 2.4: Ice volume in blue (left axis) and area in grey (right axis) of Triftglacier for the period of 1915-2023 (data from VAW Zurich).

In Figure 2.5, the mass balance for the Triftglacier is shown for each year. A value below the zero line indicates that the glacier lost volume in that year and that the summer melting process could not be compensated for by winter ice accumulation. This graph confirms the previously mentioned trend that the glacier's decline has intensified since the 1980s, as almost no year since then has shown a positive mass balance.

2.1.2 Geology

In the field of geology, information is only available on the rocks surrounding the glacier. No data on the bedrock beneath the glacier is provided in the material provided by the Swiss Federal Office of Topography (hereinafter referred to as Swisstopo). Regarding the origin of rocks within the watershed, magmatic rocks, including volcanic and plutonic types, are predominant. In terms of rock groups, crystalline rocks are dominant. The lithology primarily consists of biotite-rich gneisses, quartzites, and amphibo-

Figure 2.5: Mass balance of Triftglacier for the last 100 years (data from VAW Zurich). The unit stands for meters of water equivalent per year.

lites. Orthogneiss and Paragneiss are also abundant (Figure A.2). According to Steinemann et al. (2021), the lithology of the «Riegel» and its immediate vicinity is characterized by banded, biotite-rich gneiss, locally known as Erstfeld gneiss. Steinemann et al. (2021) also stated that, in higher areas around Hinter Tierberg (3444 m.a.s.l.), amphibolites are exposed, which is consistent with the information found in the maps of Swisstopo. In Table 2.1, the chemical composition is depicted for the most abundant rock types. Data were downloaded from the GEOROC database[1] on 13 November 2023, using the respective rock name as an indicator.

Rock Type	**SiO_2** (%)	**Al_2O_3** (%)	**FeO** (%)	**MgO** (%)	**K_2O** (%)
Biotite-rich Gneiss	30-70	15-20	*n.a.*	*n.a.*	5
Quartzite	60-90	5-15	5	*n.a.*	*n.a.*
Amphibolite	30-60	10-20	5-15	5-15	*n.a.*
Orthogneiss	50-80	10-20	*n.a.*	*n.a.*	5
Paragneiss	40-70	10-20	*n.a.*	1-5	*n.a.*

Table 2.1: Chemical composition of dominant rock types. For some compositions, no values could be found (marked with *n.a.*) meaning that these elements are not abundant in that rock type.

Except for Amphibolite, all of the rock types have similar chemical compositions, characterized by Silicon- and Aluminumoxide. The origin of the Amphibolite in the catchment is marked in Figure A.2. From the table, one can see that Silicon is the dominant element, followed by Aluminium, Magnesium, Iron, and Potassium in descending order of importance.

[1] https://georoc.eu/

2.1.3 Hydrology

The watershed for Triftsee is depicted in Figure 2.3. Data for the watershed was taken from the website of the Hydrological Atlas of Switzerland (HADES, 2023). The area covers 33.5 km^2 with an average elevation of 2663 m.a.s.l. The watershed is predominantly composed of glaciers, accounting for 58% of its coverage, followed by rock at 35%, and vegetation with only 3% (HADES, 2023).

The annual precipitation is illustrated in Figure 2.6. The graph shows that precipitation is rather constant over the year. Nevertheless, winter precipitation will fall in the form of snow, and is therefore temporarily stored, only flowing out in the summer.

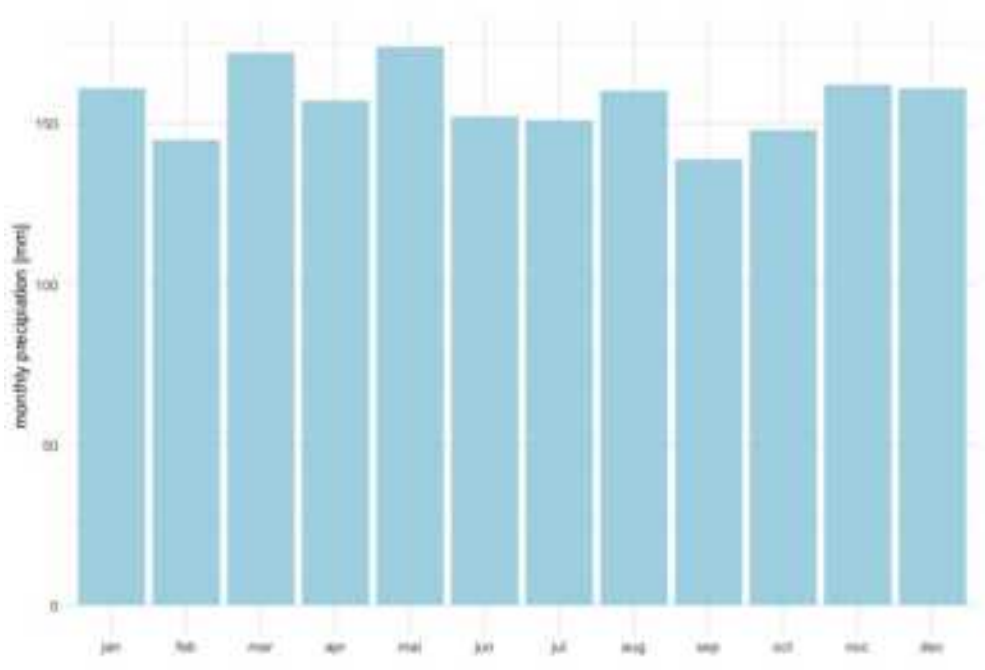

Figure 2.6: Mean precipitation over the year for the catchment of Triftsee. Yearly sum: 2201 mm. Data based on average values of the years 1981-2010 (HADES, 2023).

Continuous discharge measurements at Triftwasser (stream that drains the Triftsee) could not be found. However, data on average monthly discharge is available. According to Swisstopo, the average annual discharge is approximately 2.86 m^3/s, and the flow regime is characterized as «a-glaciare». This regime is characterized by significant differences in discharge between the winter and summer half-year, with the peak discharge occurring after the summer due to glacier melt dominance (HADES, 2023). These trends are

also evident in the monthly discharge data for Triftwasser (Figure 2.7).

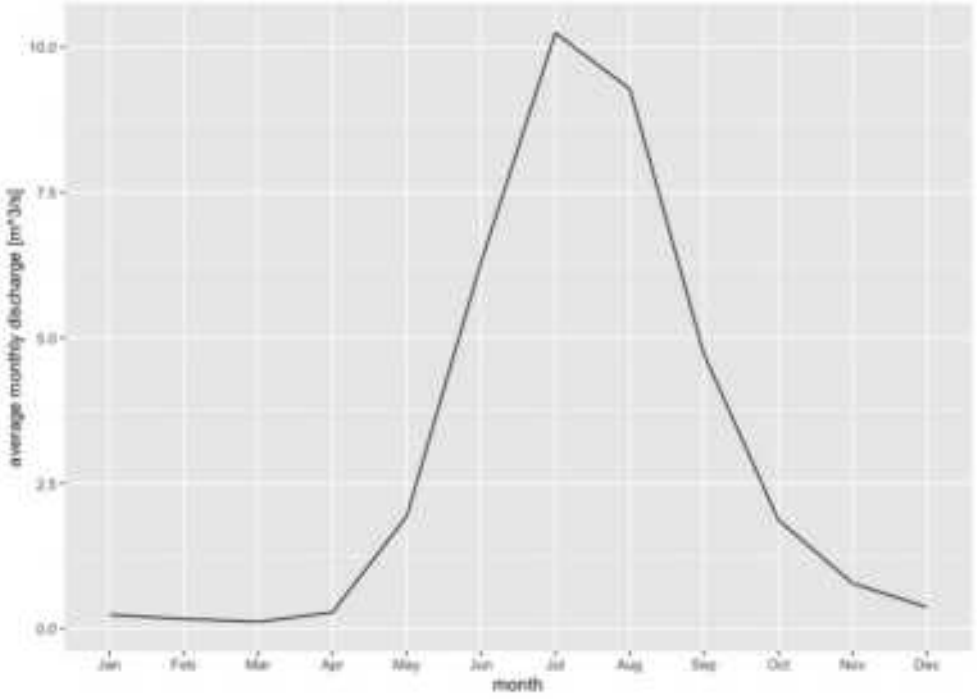

Figure 2.7: Average discharge over the year for Triftwasser. Data is based on average values from 1981-2010 (HADES, 2023).

2.1.4 Hydropower Project

The construction of a reservoir is planned in the Trift hydropower project by Kraftwerke Oberhasli AG (KWO). This reservoir should be created by erecting a 330-meter-long and maximum 177-meter-high dam in the vicinity of the suspension bridge at the end of the Triftsee, achieving a dam height of 1767 m.a.s.l. This would correspond to a usable water volume of 85 million cubic meters. A roughly 2-kilometer-long penstock would then convey the water to the planned Trift power station, situated in the vicinity of the existing water intake "Underi Trift," below the mountain station of the cable car, utilizing a head drop of approximately 425 meters. Subsequently, the water could be directed through existing tunnels to either the Hopflauenen power station or the Handeck power station, where it would be utilized in a subsequent stage for electricity generation. The project would have a construction period of around 8 years and costs of approximately 387 million Swiss Francs (Gisler et al., 2020).

2.1.5 Field Work

To address the research questions, a series of coring campaigns were conducted. The primary objective was to obtain multiple sediment cores from each lake and to perform bathymetry surveys utilizing a HyDrone. A gravity hammer corer (UWITEC) was used to retrieve the sediment cores. The samples were taken from a small, inflatable boat (Figure 2.8).

Figure 2.8: Preparing the boat and the equipment for sampling on Triftsee (Credits: Georg Odermatt).

The fieldwork at Triftsee took place on the 18th of August 2023. Alongside a team of fellow scientists from Eawag, ETH Zurich and Uni Basel, the Swiss Military facilitated our transport to the lake via helicopter from Dübendorf airport. Regrettably, there was insufficient space available to transport the HyDrone to the lake, resulting in the inability to conduct bathymetry sampling. We utilized an echosounder to approximate the lake's deepest point. The compacted and compressed nature of the sediment presented a formidable challenge in extracting sediment cores of adequate length. The first core was lost during retrieval. Subsequent attempts involved the use of a «core catcher» attached to the bottom of the tube to help retain the sediment while getting it back from the ground of the lake up to the surface. However, these efforts were unsuccessful, as we couldn't properly hammer

the core into the sediment and only water was retrieved. Ultimately, we successfully obtained a sediment core of reasonable length (table 2.2.4). Although the initial plan included sampling at the lake's outlet and near the delta, these efforts were abandoned due to the aforementioned challenges, time constraints, and the need to return via helicopter, resulting in the acquisition of only one 36-cm long core from Triftsee.

2.2 Gries

Griessee, situated at an elevation of 2386 m.a.s.l, is one of the highest reservoirs in Switzerland. Until 1958, the location was characterized by the extent of a glacier, as documented in the image in the appendix (A.6). It was in 1966 that the construction of the lake and the associated dam was completed. The dam features the following technical specifications (Baumer, 2015):

- Height: 60 meters
- Crest length: 400 meters

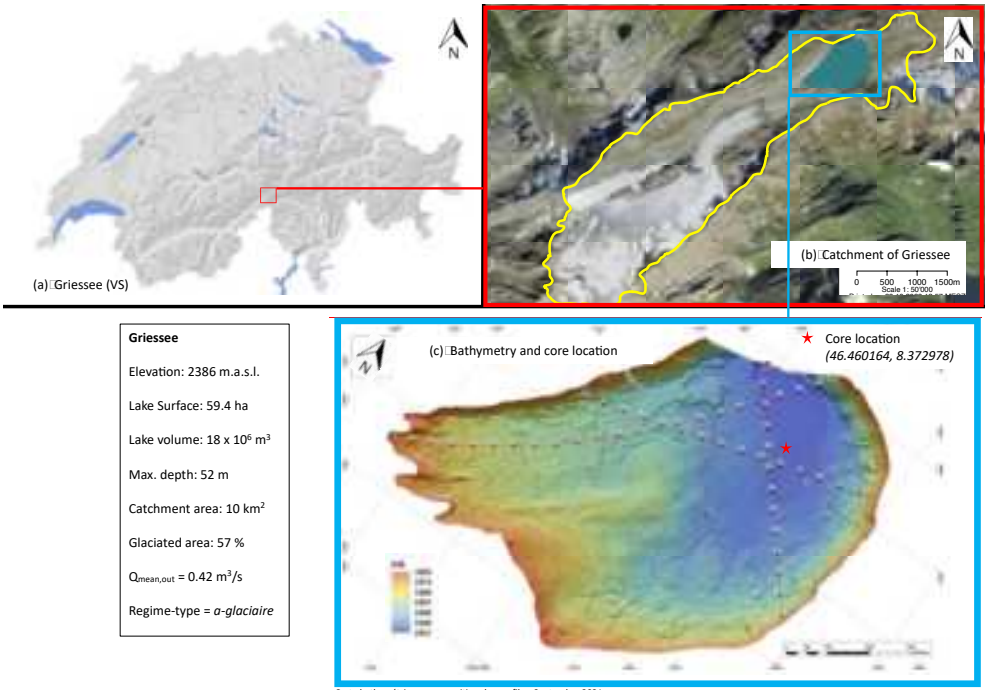

Figure 2.9: Location of Griessee on the topographical map of Switzerland together with catchment on aerial photograph. Current lake bathymetry of Triftsee was measured in 2023 by RBR Geophysics.

The hydropower station associated with Griessee is known as Altstafel and has an installed capacity of 9.7 MW, with an as-built flow rate of 2.8 m^3/s at

the gross head of 411 meters when the reservoir is at full capacity (Baumer, 2015).

The lake itself spans an area measuring 900 meters in length and 600 meters in width, with a maximum depth of approximately 60 meters. The bathymetry of Griessee is depicted in Figure 2.9.

2.2.1 Glacier

The current thickness of the glacier reaches over 500 meters and averages around 200 meters (Figure A.5). Before 1986, the Gries glacier tongue extended to the reservoir. However, since that time, it has undergone significant retreat, revealing an expanding proglacial area that now separates the glacier tongue from the reservoir (Delaney et al., 2017). In Figure 2.10, the ice volume and area of the Gries Glacier for the past hundred years are depicted. These data have also been provided by the VAW of ETH Zurich. The reduction in volume and area for the Gries glacier has remained relatively constant over nearly a century and does not exhibit a pronounced acceleration in decline since the 1980s, as observed in the case of the Trift Glacier.

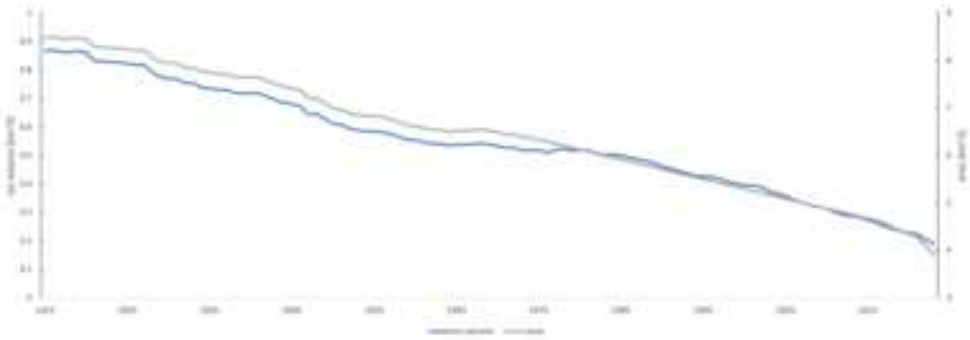

Figure 2.10: Ice volume and area of Griesglacier for the last 90 years. Data from VAW.

This pattern is further evident in Figure 2.11, where the mass balance for the Gries Glacier is presented. Almost every year of the past century has been characterized by a negative mass balance, except for a few years showing an increase between 1960 and 1980.

2.2.2 Geology

The data situation was similar to that of Triftsee, with geological information only available for areas not covered by the glacier. The following data was obtained through the consultation of Swisstopo. The geomorphology of the catchment area has been notably shaped by glacial processes during the Ice Age, contributing to the unique geological features of the lake. Griessee is surrounded by a diverse range of rocks, primarily composed of biogenic

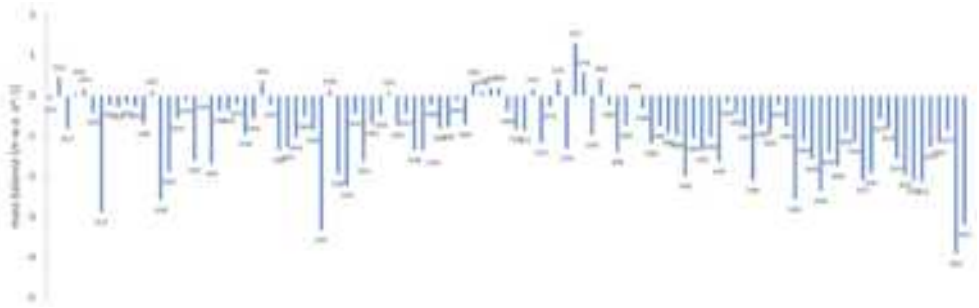

Figure 2.11: Mass balance of Griesglacier for the last 100 years. The unit stands for meters water equivalent per year. Data from VAW.

and clastic sedimentary rocks, as depicted in the image A.7 provided in the Appendix. These rocks belong to the group of sedimentary rocks with dominant lithologies including Marl shale (≪Mergelschiefer≫) and some dolomite, as visually represented in the image (A.8). Also Breccia, Marble, Conglomerate, Claystone and calcitic rocks (such as calcareous shale, detrital limestone, and marly limestone) are present. In Table 2.2, the chemical composition is depicted for the most abundant rock types. As for Trift, data were downloaded from the GEOROC database[2] on 13 November 2023, using the respective rock name as an indicator.

Rock Type	**SiO_2** (%)	**Al_2O_3** (%)	**Fe_2O_3** (%)	**CaO (%)**	**MgO (%)**	**K_2O** (%)
Dolomite	5-30	*n.a.*	5	30-50	10-20	*n.a.*
Breccia	30-50	10-20	5	*n.a.*	*n.a.*	*n.a.*
Marble	30-50	10	*n.a.*	30-50	20	10
Conglomerate	50-70	10	10	*n.a.*	*n.a.*	5
Claystone	30-60	20	10	1-10	1-10	*n.a.*
Marl shale	16	14	4	22	1	*n.a.*

Table 2.2: Chemical composition of dominant rock types. For some compositions, no values could be found (marked with *n.a.*) meaning that these elements are not abundant in that rock type.

Also in this context, Silicon stands out as the predominant element in the lithology of the catchment. Additionally, there is a notable abundance of Calcium, followed by Aluminum, Magnesium, Iron, and Potassium in decreasing order of significance.

[2]https://georoc.eu/

2.2.3 Hydrology

The catchment area encompasses approximately 10 km^2 and exhibits an average elevation of 2771 m.a.s.l (Figure 2.9). The dominant land cover types within the catchment area are as follows: glaciers, covering 57%; rocks, accounting for 27%; loose sediments, representing 9%; and water, making up 6%.

While annual precipitation data for the station directly below the reservoir is not available (because the catchment is too small), data from the station «Ägene Obergoms» further downstream in the valley indicates an annual runoff of 1639 millimeters, as shown in Figure 2.12.

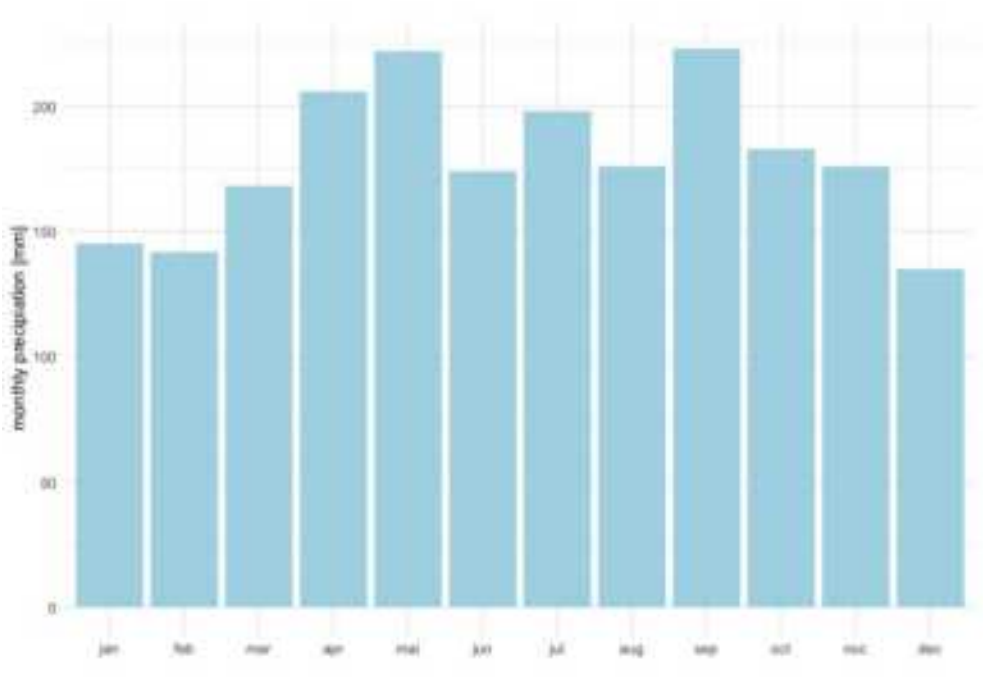

Figure 2.12: Mean precipitation over the year for the catchment of «Ägene Obergoms». Data are average values from 1981-2010(HADES, 2023).

The lake's discharge regime falls under the category of «a-glaciaire», characterized by significant seasonal variations in flow. The average annual discharge rate is approximately 0.42 m^3/s, with Figure 2.13 illustrating the seasonal discharge trends. However, it's worth noting that a substantial portion of Griessee's water is (after passing through the power station Altstafel) directed through a tunnel to the canton of Tessin for further hydroelectric power generation, resulting in smaller seasonal variations and total discharges for the downstream section.

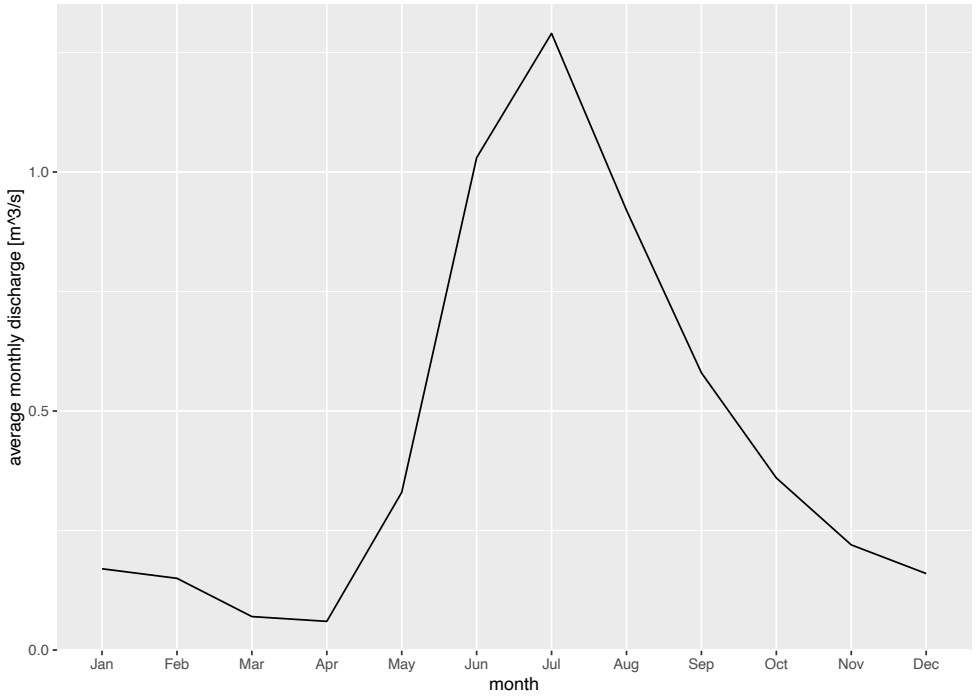

Figure 2.13: Average discharge over the year below the reservoir. Data are average values from 1981-2010 (HADES, 2023).

2.2.4 Field Work

Fieldwork for Griessee was conducted on August 30, 2023. Similar challenges, as described for Triftsee, were encountered. The sediment in Griessee was highly compact, making it difficult to extract sediment cores. Consequently, only one sediment core of adequate length (45 cm) could be successfully retrieved (see Table 2.2.4).

Table 2.3: Data of the retrieved sediment cores.

Name	Coordinates (LV95)	Depth of location	Length of core
23_TRIFT	1171450.015, 2670369.746	43.7 m	36 cm
23_GRIES	1145852.663, 2671775.951	38.1 m	45 cm

Chapter 3

Methods

Laboratory work was conducted at the Swiss Federal Institute for Aquatic Research (Eawag) in Dübendorf. Each sediment core was split lengthwise using a Geotek core opener. One half was archived at 4 degrees Celsius for future reference (Figure 3.1), while the other half was designated for several analyses: line scan, XRF core scanning, grain size distribution, bulk density measurements, and gamma spectroscopy.

3.1 Line Scan

A two-dimensional photo of each core was taken utilizing a JAI LT-400 CL-F Color Line Scan Camera attached within the Avaatech micro XRF core scanner. This advanced camera system can generate high-resolution color images of sediment cores. These images enable the visual analysis of the annual layers or sedimentary bands. To enhance visibility and clarity, the working halves of the cores were stationed and let oxidize to significantly enhance the visibility of laminations and other features within the sediment core.

3.2 XRF Analysis

The utilization of XRF core scanners gained substantial popularity in the last decade due to their ability to non-destructively extract elemental intensities from sediment cores with minimal analytical effort (Weltje & Tjallingii, 2008). In contrast to conventional geochemical analyses, this method enables the acquisition of high-resolution data within short time frames, typically spanning from hours to days. Consequently, this approach facilitates the creation of detailed time-series data for major elements, which can be applied to paleoclimate and paleoenvironmental interpretations (Zolitschka et al., 2015).

Figure 3.1: Image of the sediment cores after splitting (left: Triftsee, right: Griessee).

The working half of the core was scanned using an Avaatech micro XRF core scanner (Figure 3.2). Before the scans, the sediment core surface was properly cleaned and leveled. An ultrafine foil was used to cover the surface of the core to avoid contamination between the scanner and the sample and to ensure proper contact with no air in between. The analysis in the Avaatech micro XRF core scanner enables the almost continuous identification of elements present in the sediment core (Boyle, 2000). Semi-quantitative elementary compositions were measured for different elements at different voltages (Table 3.1). The core was subjected to 3 different settings to determine elemental composition downcore: 10 kV at 15 seconds count time, 30 kV at 40 seconds count time, and 50 kV at 40 seconds count time.

Figure 3.2: Avaatech micro XRF core scanner in the lab of Eawag for XRF analysis.

It's important to note that the data output is expressed in semi-quantitative elementary concentrations, specifically as counts per unit time (e.g. CPS, counts per second). The time therefore expresses how long the sediment was bombarded with energy sources. These measurements cannot be linearly converted into quantitative metrics unless with a known external standard or by wet chemistry on an ICP-MS (inductively coupled plasma mass spectrometry).

Table 3.1: Elements measured in the XRF Analysis by acceleration voltage.

10kV	Mg, Al, Si, P, S, Cl, Ar, K, Ca, Ti, V, Cr, Mn, Fe, Co
30kV	Ni, Cu, Zn, Ga, As, Br, Rb, Sr, Y, Zr, Mo, Rh, Pb, U
50kV	Ba, Ag

After the scan, the half core was subsampled every centimeter for dry-bulk density and water content, and every half centimeter for grain size analysis.

3.3 Grain Size Analysis

Pea-sized sediment samples were taken with a spatula from the working half of the core every half centimeter to determine the grain size distribution. These subsamples were suspended in Calgon, in 10ml plastic tubes, and placed overnight on an overturning shaker before measurements. Calgon is

used because it is a dispersing agent, which helps to prevent the particles from sticking together and therefore prevents aggregation, allowing better results for the grain size distribution. The grain size distribution in each sample was determined using the LS 13 320 XR Laser Diffraction Particle Size Analyzer (Figure 3.3). This analysis provided the grain size distribution, specifically referring to clay (smaller than 0.002 mm), silt (between 0.002 and 0.05 mm), and sand (bigger than 0.05 mm) particles.

Grain size analysis provides insights into the intensity of discharge, with larger grain sizes indicative of more intense discharge. Conversely, smaller grain sizes are associated with less intense discharge.

Figure 3.3: Photo of LS 13 320 XR Laser Diffraction Particle Size Analyzer (Beckman & Coulter) used for the analysis.

3.4 Dry Bulk Density and Water Content

At every 1-centimeter depth interval, a 1 cm^3 volume of sediment was taken from the sediment core (Figure 3.4) using a defined 1 cm^3 volumetric sampler. The sample was weighed before and after freeze-drying. This procedure enabled the calculation of both the dry bulk density (3.1) and the water (3.2) content.

$$\rho_d = \frac{m_d}{V_t} \tag{3.1}$$

This formula calculates the dry bulk density (ρ_d), representing the mass of dry soil (m_d) per unit volume (V_t).

$$\theta = \frac{m_w}{m_d} \times 100\% \tag{3.2}$$

The water content (θ) is determined by the ratio of the mass of water (m_w) to the mass of dry soil (m_d), expressed as a percentage.

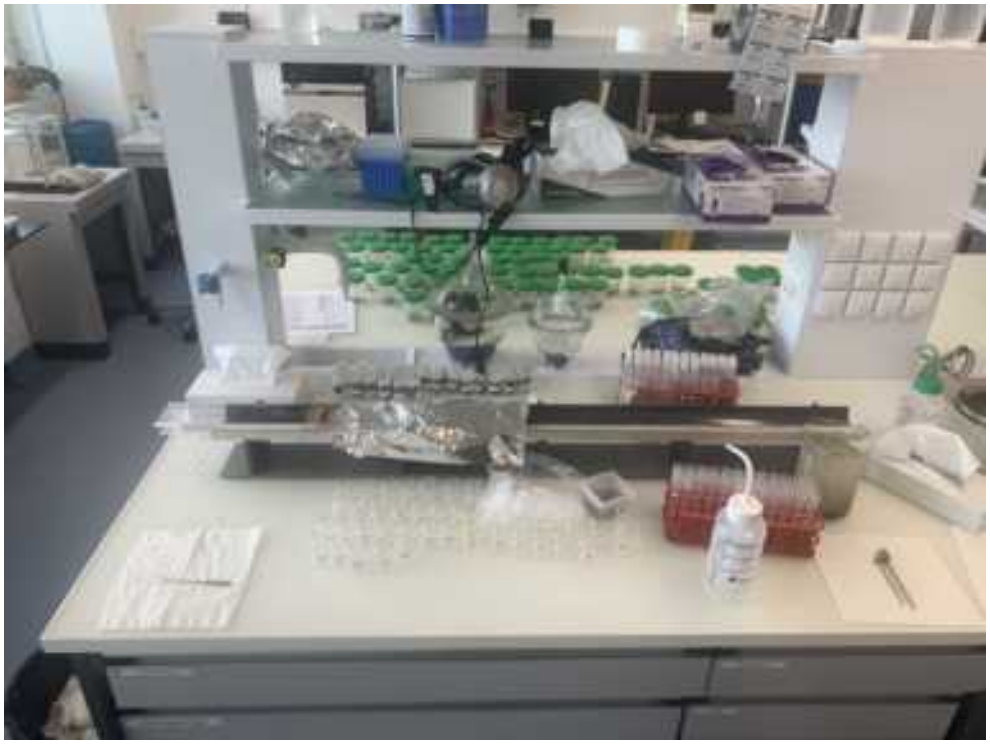

Figure 3.4: Preparing the samples for dry-bulk density, grain size analysis and gamma spectroscopy.

3.5 Gamma Spectroscopy

The rest of the samples were ground using a mortar and pestle, transferred to a tube, and left to equilibrate for two weeks before being subject to gamma spectroscopy (Putyrskaya et al., 2015). The duration of analysis for each sample was approximately two days.

The dating process relied on short-lived isotopic chronometers, focusing on three distinct isotopes: Lead (^{210}Pb), Cesium (^{137}Cs), and Beryllium (^{7}Be). The measurements were carried out using Germanium-well detectors (Canberra Industries) at Eawag Dübendorf.

Lead-210 (^{210}Pb), a natural geogenic radioisotope, has a half-life of 22.3 years. It is a naturally occurring isotope in the ^{238}U decay series. It is produced

when ^{226}Ra in rocks and soils decays to ^{222}Rn, which then escapes to the atmosphere and decays into ^{210}Pb (Matisoff & Whiting, 2011). This isotope has a residence time in the atmosphere of around 10 days before deposition through precipitation onto the lake sediments. The analysis of ^{210}Pb involves measuring supported and unsupported forms. Unsupported ^{210}Pb, originating from atmospheric decay, decreases over time downcore, which allows the estimation of sedimentation rates over the last 100-150 years. The calculations are based on the CF-CSR (constant flux - constant sedimentation rate) model. As the name indicates, this model assumes that the flux of ^{210}Pb into the sediment surface and the sedimentation rate is constant over a certain interval of time and depth. This assumption leads to a constant concentration of the unsupported ^{210}Pb in the surface sediment. Therefore, the vertical distribution of the unsupported ^{210}Pb in the sediments can be described as:

$$C(x) = C(0) \cdot e^{-\frac{l \cdot w(x)}{Rs}}$$

where $w(x)$ is the cumulative weight of sediments above the depth x in g/cm^2, Rs is the mass sedimentation rate in g/cm^2/yr and l is the decay constant for ^{210}Pb. By employing an exponential fit to the unsupported ^{210}Pb data, the value of Rs can be determined. In this case, the age of the sediment layers, denoted as $t(x)$ in years, can be calculated as:

$$t(x) = \frac{w(x)}{R_{s,const.}}$$

The presence of ^{210}Pb is important in dating sediment and soil processes, especially in lakes dominated by atmospheric fallout (Kumar et al., 1999). Unsupported ^{210}Pb becomes negligible after 150 years. Its concentration in sediment records follows an exponential decrease, giving insights into sedimentation rates. It is more applicable for dating sediment cores in lakes with low sedimentation rates and undisturbed watersheds, where the influx of contaminants is mostly influenced by atmospheric fallout (lakes characterized by atmospheric dominance).

Beryllium-7 (^{7}Be) is a naturally occurring cosmogenic nuclide, generated through cosmic ray interactions with atmospheric nitrogen (^{14}N) and oxygen (^{16}O). This process is called spallation. It is introduced to Earth through precipitation, with high reactivity and rapid association with sedimentary substrates. With a half-life of only 53 days, which gives an effective range of approximately 6 months, the presence of ^{7}Be in a sample indicates recent contact with the atmosphere, making it a key factor in dating with ^{210}Pb because it shows if really the most recent sediment was caught (Mabit et al., 2008).

Cesium-137 (^{137}Cs) is an artificial radionuclide, resulting from thermonuclear activities such as nuclear bomb tests and accidents at nuclear power plants (like Chernobyl and Fukushima). With a half-life of 30.3 years, ^{137}Cs serves as an event dating technique, offering a marker for specific events within the last 100 years. It is both a pollutant and a tracer, particularly helpful in high-sedimentation-rate settings (Christoudias & Lelieveld, 2013).

3.6 Mass Accumulation Rate

The mass accumulation rate can be calculated after having measured the dry-bulk density and having determined a sedimentation rate with equation 3.3.

$$MAR = \rho_d \times Rs \tag{3.3}$$

In this formula, MAR represents the mass accumulation rate, ρ_d is the dry bulk density, and Rs is the sedimentation rate. The sedimentation rate (Rs) is a parameter representing the rate at which sediment accumulates, typically measured in centimeters per year (cm/a).

Chapter 4

Results

4.1 Line Scan

Figure 4.1 below shows the line scan image generated for both Triftsee and Griessee. The Triftsee core shows visible laminations from the top to around 20 cm. On the other hand, the Griessee sediment core has no such evident laminations. In Triftsee, the layers remain relatively horizontally arranged in the upper 10 centimeters, but beyond 10 centimeters, they exhibit some lateral displacement, and further below, they are no longer distinct. This might be due to coring artifacts. The results from other analyses (dry-bulk density, gamma, grain size, XRF) will aid in determining whether the laminations in Triftsee represent individual events or entire years (then being referred to as varves) and whether, despite visual homogeneity, trends can be identified in the data for Griessee.

4.2 XRF Analysis

All measured elements were plotted against depth, and the data was examined to identify patterns or trends while distinguishing them from random fluctuations, often referred to as white noise. For the elements that displayed clear trends, a correlation table was computed (Table 4.1 and 4.2). The focus was on elements that could be linked to grain size analysis and to dry bulk density, as well as to terrestrial and mineralogical input and photosynthetic activity. Silicon (Si) and Aluminium (Al) were plotted for both Gries- and Triftsee, because these elements are dominant in the lithologies of the catchment, as described in the section 2.2.2 of Trift and 2.2.2 of Gries. Although Magnesium (Mg) is also abundant in the catchment of Griessee, it was not included in the correlation table, because the results for Mg for the XRF Analysis showed white noise behavior. Rubidium (Rb) was also included because literature compilations indicate average claystones and siltstones typ-

Figure 4.1: Line scan for Griessee (left) Triftsee (right).

ically demonstrate enrichment in Rb. Strontium (Sr) was included because, in sedimentary sequences, Sr is typically found in association with carbonate minerals, specifically calcite, and aragonite, owing to the substitution of Sr for Calcium (Ca) within the carbonate lattice (Fralick & Kronberg, 1997). Additionally, Sr may be present in association with biotite, although at significantly lower concentrations than observed in carbonate minerals(Fralick & Kronberg, 1997). It should also be mentioned that Titanium (Ti) was not included for Griessee, as the CPS values exhibited white noise behavior rather than a clear trend.

Table 4.1: Correlation table for the elements in the catchment of Griessee.

	Al	Si	K	Ca	Fe	Rb	Sr	Ba	Ag
Al	1								
Si	0.39	1							
K	0.48	-0.46	1						
Ca	0.48	0.49	0.26	1					
Fe	0.25	-0.64	0.92	0.14	1				
Rb	0.09	-0.75	0.82	-0.09	0.92	1			
Sr	0.04	0.46	-0.12	0.58	-0.14	-0.2	1		
Ba	-0.06	-0.7	0.66	-0.15	0.77	0.86	-0.12	1	
Ag	0.43	-0.13	0.43	0.21	0.46	0.41	0	0.22	1

The correlation tables represent correlations with colors that denote the strength of these relationships. Moderate trends, with correlation coefficients ranging from 0.5 to 0.7 (absolute values), were represented in yellow, while strong trends, with correlations from 0.7 to 0.99 (absolute values), were indicated in red (Table 4.1 and 4.2). It's important to note that the correlation of an element with itself is always 1, found along the diagonal entries in the table.

In Griessee, a total of seven strong correlations were identified among various elements, indicating significant relationships in their CPS values. Additionally, three moderate trends were observed, showing less pronounced but still meaningful connections between elements. It's worth mentioning that these trends were primarily associated with elements of moderate atomic weight. Shifting our focus to Triftsee, a slightly different pattern emerges. In this lake, eight strong trends were identified among elements, signifying substantial associations between their CPS values. Four moderate trends were observed, indicating less pronounced yet still notable relationships between elements. Notably, these trends in Triftsee were more frequently linked to elements with lighter atomic weights.

For further analysis, the CPS values were standardized to facilitate a more effective visual comparison (Equation 4.1). As described in chapter 3.2, the focus is not on quantitative values but rather on identifying trends when analyzing the XRF output data.

$$\mathrm{El}_{\mathrm{cps,std}} = \frac{\mathrm{El}_{\mathrm{cps}} - \mu_{\mathrm{El,cps}}}{\sigma_{\mathrm{El,cps}}} \tag{4.1}$$

In this formula, the standardized value of the CPS value for an element ($\mathrm{El}_{\mathrm{cps,std}}$) is equal to the CPS-value ($\mathrm{El}_{\mathrm{cps}}$) minus the mean average CPS value

Table 4.2: Correlation table for the elements in the catchment of Triftsee.

	Al	Si	K	Ca	Ti	Fe	Rb	Sr	Ag	Ba
Al	1									
Si	0.91	1								
K	0.89	0.74	1							
Ca	0.34	0.52	0.23	1						
Ti	0.74	0.73	0.75	0.6	1					
Fe	0.65	0.48	0.77	0.35	0.8	1				
Rb	0.44	0.21	0.6	-0.29	0.21	0.44	1			
Sr	-0.31	-0.08	-0.45	0.48	-0.19	-0.42	-0.71	1		
Ag	0.12	0.17	0.16	0.12	0.32	0.28	-0.11	-0.02	1	
Ba	0.42	0.38	0.5	0.23	0.42	0.36	-0.07	0.14	0.42	1

($\mu_{\mathrm{El,cps}}$) divided by the standard deviation of the CPS value ($\sigma_{\mathrm{El,cps}}$). Standardized values are graphed for elements that display pronounced depth-related trends, both adjacent to the line scan (Figure 4.2 and 4.3). These figures also include plots of significant and distinctive element ratios. The element ratios were calculated with the original CPS values and not with the standardized ones. In grey, interesting depths with peaks are marked.

For Triftsee, the standardized CPS values for the elements Aluminum (Al), Potassium (K), Iron (Fe), and Titanium (Ti) were plotted together with depth next to the line scan due to their notable trends identified in the correlation table. Visually, it is apparent that their respective lines closely align. Additionally, the ratios of Barium to Silicon (Ba/Si) and Silicon to Titanium (Si/Ti) were computed, as these represent characteristic elemental ratios commonly employed in other XRF analyses. Although other characteristic elemental ratios were considered, they exhibited white noise behavior rather than clear trends.

Four distinctive depths were identified. At approximately 6 and 16 centimeters, the standardized values of the individual elements, along with the Si/Ti ratio, display peaks in the opposite direction to the peaks observed for the Ba/Si and Si/Al ratios. Around the depth of 21 centimeters, the most prominent peaks emerge, reflecting trends similar to those observed at shallower depths. However, at this depth, the Si/Ti ratio aligns its peak with the trends exhibited by the other ratios. Similarly, at a depth of around 35 centimeters, analogous trends and peaks as described for the 21-centimeter depth become apparent.

For Griessee, the standardized CPS values of Rubidium (Rb), Silicon (Si), Potassium (K), Iron (Fe), and Barium (Ba) are plotted together with depth next to the line scan because they exhibit similar trends (except Si, which shows an inverse trend). Additionally, Rb and Strontium (Sr) are plotted together because they display trends in opposite directions. In this case,

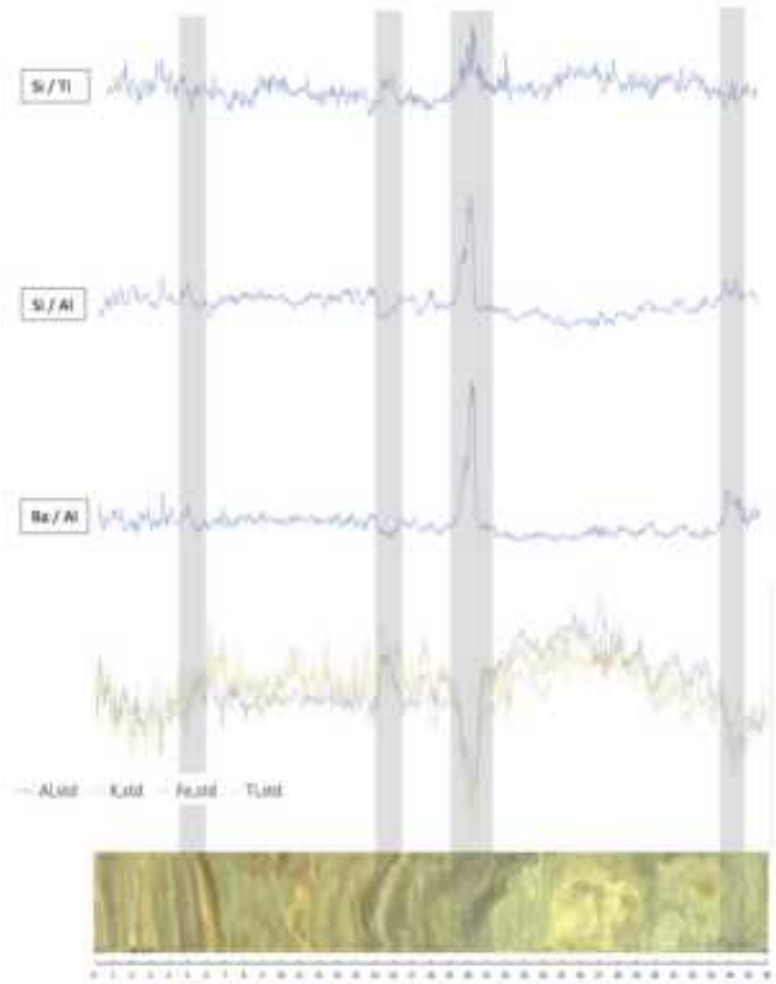

Figure 4.2: Standardized CPS values for selected elements and important element rations for Triftsee with depth plotted next to the line scan.

only the elemental ratios of Si to Aluminum (Al) and Ba to Al are plotted, as the ratio Si/Ti showed white noise rather than clear trends.

Two noteworthy depths were identified for Griessee. At a depth between 1 and 2 centimeters as well as between 7 and 9 centimeters, there are peaks in the same direction for the ratios Si/Al, Ba/Al, and the individual element Ba. The other elements — Rb, Si, K, and Fe — exhibit peaks in the opposite direction, and Rb and Sr show no discernible peaks at all. At a depth between 7 and 9 centimeters, a peak in the same direction for both elemental ratios can be identified, which is opposite to the peaks for the individual elements Si and K. The other elements do not show peaks at that depth. There are some peaks at a depth between 25 and 35 centimeters for Si/Al, which are not represented in the other graphs. Rb and Sr show several peaks with

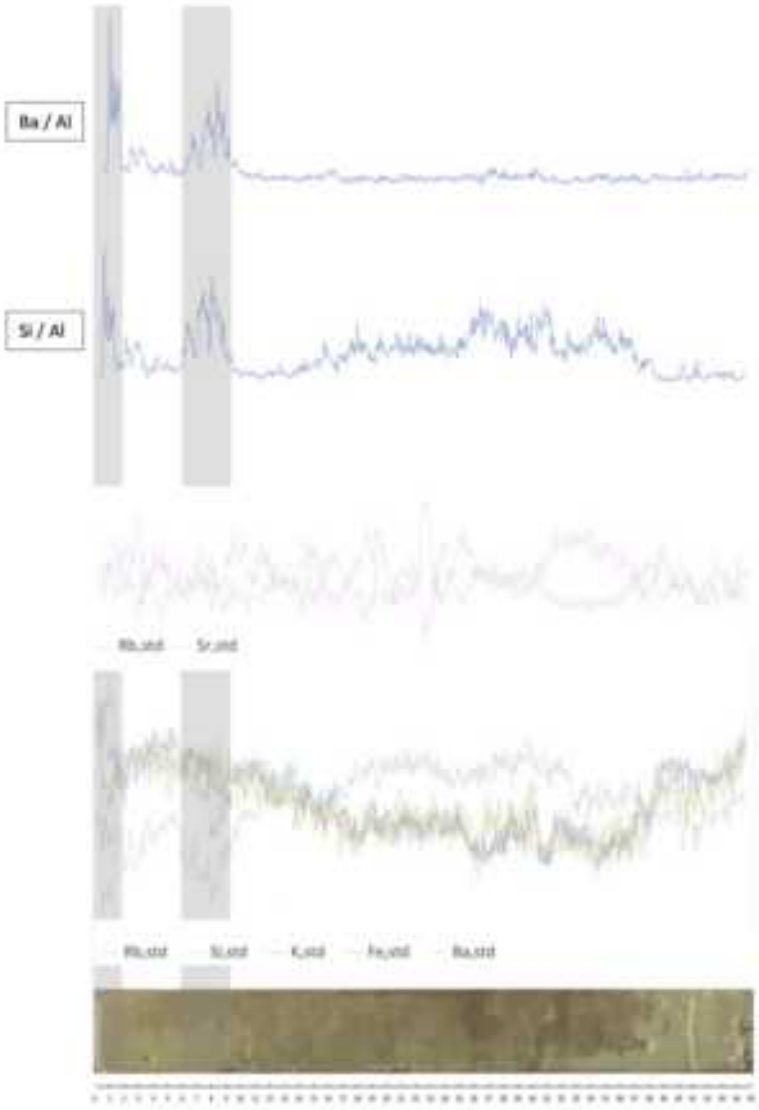

Figure 4.3: Standardized CPS values for selected elements and important element rations for Griessee with depth plotted next to the line scan.

depth, none of which correspond with peaks in the other single elements or element ratios.

Also, the ratio of Al/Ti and Si/Ti were plotted together with depth because they can potentially be linked with terrestrial input (Myrstener et al., 2021). Al and Ti are both terrigenous input proxies, an increase in concentration means more material is coming in (Myrstener et al., 2021). Normalization with Ti means looking at provenance or source (Myrstener et al., 2021). Therefore, between depths of 5 and 10 centimeters as well as between depths

between 40 and 45 centimeters, there could potentially be a higher terrestrial input for Griessee (Figure 4.4).

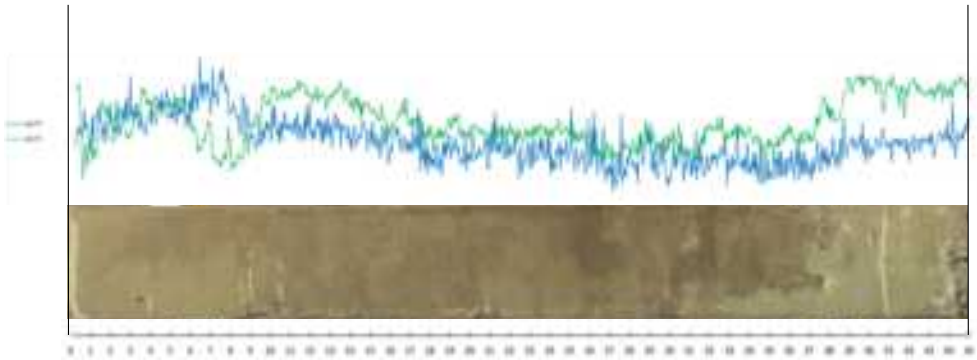

Figure 4.4: Ratios of Al/Ti and Si/Ti for Griessee.

For Triftsee, there is a peak at around 20 cm depths (Figure 4.5), which could potentially correspond to a higher terrestrial input.

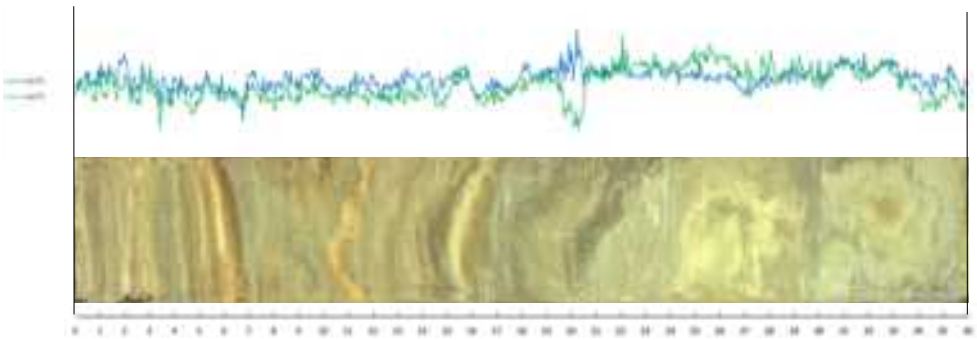

Figure 4.5: Ratios of Al/Ti and Si/Ti for Triftsee.

The dominant elements differ between the two lakes: In Griessee, the most influential elements, in order of importance, are Calcium, Iron, Silicon, and Potassium, as evidenced by the highest CPS values. In Triftsee, the dominant elements, in the following order, are Iron, Silicon, Silver, and Potassium, also characterized by the highest CPS values.

4.3 Grain Size Analysis

The results for the grain size analysis are depicted in Figures 4.6 and 4.7 for the two sediment cores. For every half centimeter, the proportion of clay, silt, and sand was measured across the entire depth. The size classes considered are clay (less than 2 μm), silt (between 2 and 62.5 μm), and sand (greater than 62.5 μm).

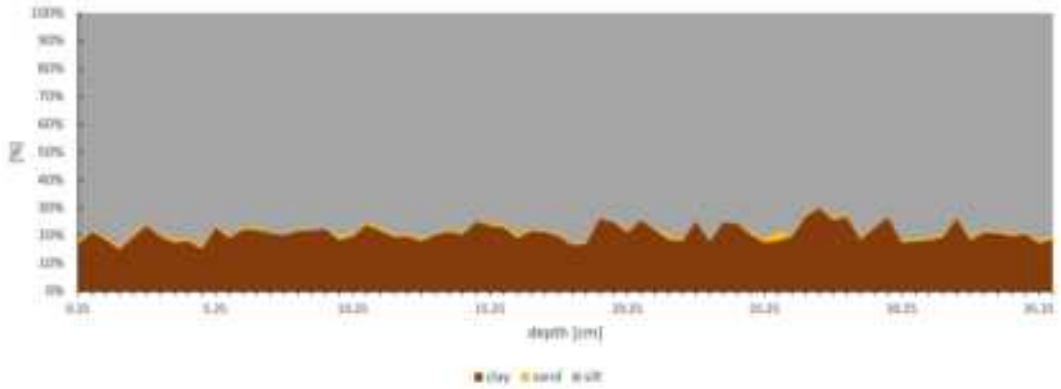

Figure 4.6: Results for grain size analysis for Triftsee.

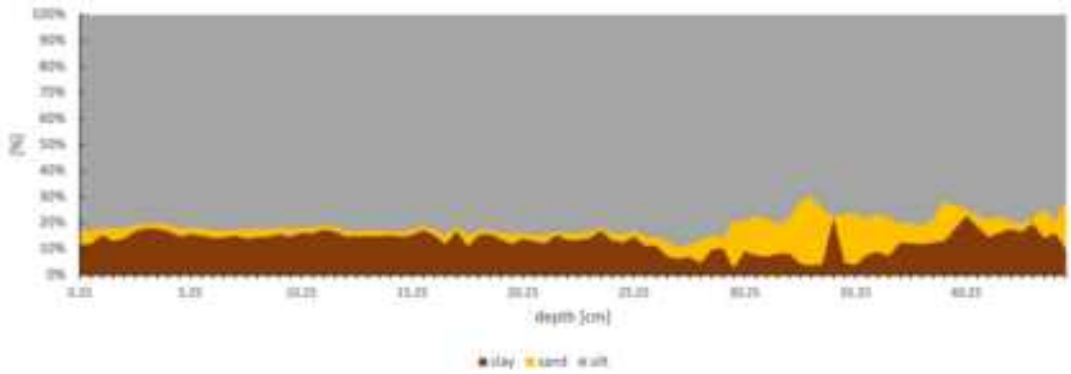

Figure 4.7: Results for grain size analysis for Griessee. The sample at a depth of 39.5 mm couldn't be measured and was therefore linearly interpolated.

For both cores, the proportion of silt is dominant and consistently around 80%. While sand also constitutes a significant portion of Griessee, it remains below one percent at all depths for Triftsee. Therefore, clay comprises almost the entire remaining proportion of 20% for Triftsee, whereas for Griessee, the clay content averages around 10%.

While the proportions for Triftsee remain relatively constant with depth, the situation differs for Griessee. Beyond a depth of 30 centimeters, the sand

content increases to approximately 20% (at a depth of 35 centimeters) and then decreases again to the initial value of under 5% by a depth of 40 centimeters. After that, the sand content increases again a bit to the final depth of 45 cm. No clear reason for this phenomenon could be identified. Potential explanations could be that the observed phenomenon is likely linked to ongoing processes within the catchment. The necessity for greater energy to transport larger grains may suggest proximity to the glacier, with intensified meltwater flow potentially responsible for transporting these specific sand grains. Alternatively, the dynamics could be influenced by the periodic flushing of the reservoir, impacting sediment transport and contributing to variations in downstream grain size distribution. However, upon examining the line scan (Figure 4.1), distinct sediment structures in that area become apparent.

4.4 Dry Bulk Density and Water Content

In Figure 4.8 and 4.9, both dry bulk density and water content are graphed together against depth. The sediment's line scan serves as the background for this representation.

In Triftsee, we observe a slight decrease in dry bulk density with increasing depth, contrary to the expectation of an increase in dry bulk density due to the additional weight from the top and therefore higher compression. However, there isn't a clear and consistent pattern when it comes to water content. Interestingly, at around 30 cm depth, we observe a brief increase in water content throughout a few centimeters before it subsequently decreases once more. This region corresponds to lower dry bulk density, affirming the trend that associates higher water content with lower dry bulk density. This suggests that sediments in this area are more porous and less dense, providing more capacity for water retention. The water content in the whole core is around 20% with a minimal value of 17.12 % at 37 cm depth and a maximal value of 47.49 % at 29 cm depth. The dry-bulk density has values of around 1.2 g/cm^3 with a minimal value of 0.53 g/cm^3 at 32 cm depth and a maximal value of 1.77 g/cm^3 around 9 cm depth. Values of dry-bulk density below 1 g/cm^3 seem a bit unrealistic because this would mean that the density would be smaller than water. An explanation could be that during retrieval of the core, water, and air were also caught in the core.

For Griessee, we don't find clear trends for either dry bulk density or water content with depth. However, we notice again the inverse relationship between the two: as dry bulk density goes up, water content tends to decrease, and vice versa. The water content in the whole core is also around 20% with a minimal value of 15.25 % at 23 cm depth and a maximal value of 25.77 % at 1 cm depth. The dry bulk density has values around 1.5 g/cm^3 with

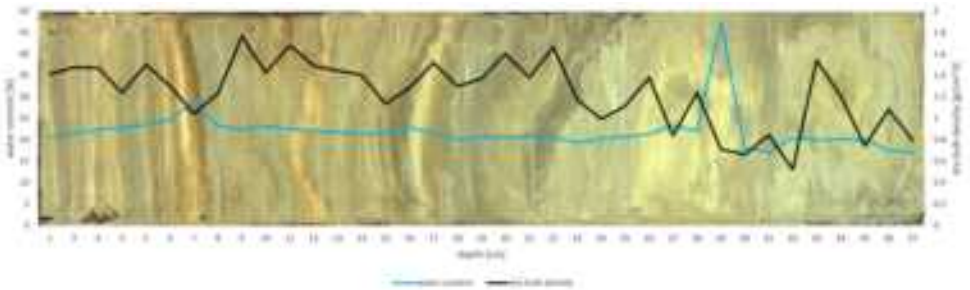

Figure 4.8: Dry bulk density and water content for sediment core of Triftsee.

a minimal value of 0.87 g/cm^3 at 2 cm depth and a maximal value of 1.98 g/cm^3 around 8 cm depth.
The study that was mentioned before by CONSULTEST SA for Griessee showed results for water content in the sediment of approximately 27 %, a finding consistent with the results from the sediment cores in this project, where the water content averaged slightly above 20 %.

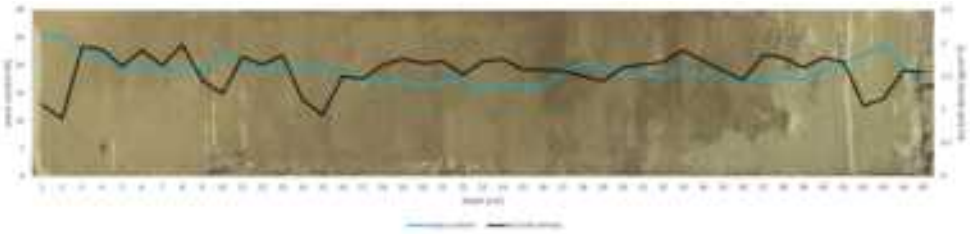

Figure 4.9: Dry-bulk density and water content for sediment core of Griessee.

In terms of result accuracy, it can be stated that these should be approached with caution. The 1 cm^3 samples were taken manually. Since the sediment was partially very hardened or very soft, not all samples were likely precisely 1 cm^3 in size. However, the value of 1 cm^3 directly contributes to the calculation of dry bulk density and water content, and therefore, it can have a significant impact on the outcome.

4.5 Gamma Spectroscopy

As described in Chapter 3.5 in the methods, activities of ^{210}Pb, ^{137}Cs, and ^{7}Be were measured. ^{7}Be was detected in the top sediment layer (depth of 0-0.5 cm) of Triftsee. Accordingly, it can be confirmed that the core indeed represents the most recent sediment. The results for ^{210}Pb and ^{137}Cs are depicted in Figure 4.10, with data points measured for every 3-5 centimeters.

The activity of unsupported ^{210}Pb decreases as expected with depth. When

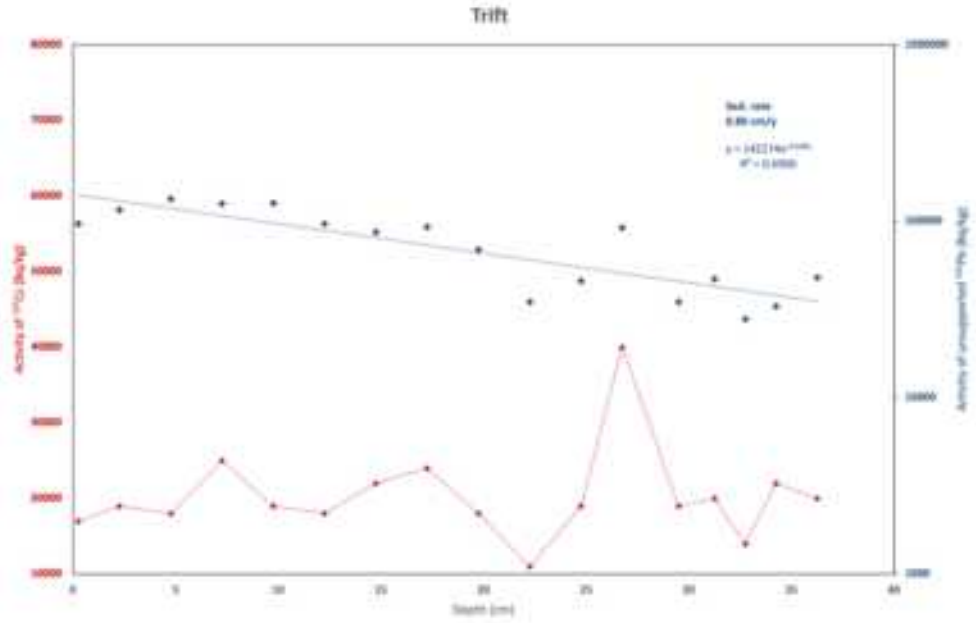

Figure 4.10: Results for the activity of ^{210}Pb and unsupported ^{137}Cs in Triftsee. The activity of unsupported ^{210}Pb plotted on a logarithmic scale.

the data points are linearly correlated (with unsupported ^{210}Pb activity plotted on a logarithmic scale), the sedimentation rate of 0.8 cm/year can be read from the slope of the line. The R-value is close to 0.7, indicating a strong correlation.

This would mean that the sediment core being analyzed is 45 years old, while the lake has only existed for the past 23 years. Lamination analysis on the line scan (see Figure 4.1) indicates clear lamination patterns, but only up to a depth of 20 cm. There is a possibility that sediment in the lake is limited to the uppermost 20 cm, with sediment below originating from glacier sedimentation before the lake's formation.

To address this, a new linear trendline was applied, considering only the range down to 20 cm depth, where laminations are present. The top data point was excluded due to potential disturbances. The resulting sedimentation rate is 0.94 cm/year with an R^2 of approximately 0.7. In practical terms, since the lake's inception, 21.6 cm of sediment has accumulated within the past 23 years, starting from the year 2000.

As for the activity of ^{137}Cs, the results for this interval are not very reliable due to the short period. However, there is a peak at a depth of 26.75 centimeters. Assuming a sedimentation rate of 0.8 cm/year, this would imply that the sediment at a depth of approximately 26.75 cm is around 33 years old, dating back to the year 1990. This is not far from the Chornobyl accident in

1986, and the peak may therefore possibly be associated with that event.

In the investigation of Griessee, the same isotopes—^{137}Cs, ^{210}Pb, and ^{7}Be—were measured. However, the detection of ^{7}Be in the uppermost sample was unsuccessful, raising uncertainty regarding whether the most recent sediment was accurately represented.

Results for ^{137}Cs and ^{210}Pb in Griessee are illustrated in Figure 4.11.

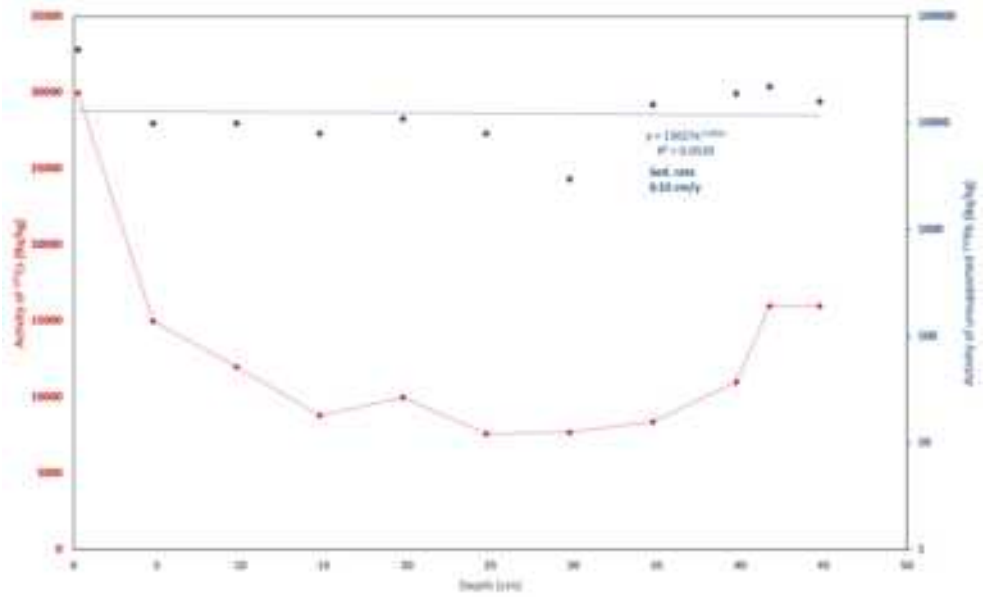

Figure 4.11: Results for the activity of ^{210}Pb and ^{137}Cs in Griessee. The activity of ^{210}Pb plotted on a logarithmic scale.

The ^{137}Cs profile exhibits a peak in the uppermost sample and another around 40-45 cm. These peaks, potentially influenced by glacier melting, pose challenges for accurate interpretation.

The ^{210}Pb levels remain relatively high, complicating the determination of an average sedimentation rate. A preliminary estimate suggests a rate of 0.55 cm/a, albeit with a low R^2 (0.0539).

Upon excluding the last four data points, a sedimentation rate of 1.94 cm/a for depths between 0 and 30 cm is derived, with an improved R^2 of 0.151. While this remains an imperfect estimate, it represents an enhancement compared to the previous calculation.

To obtain an accurate sedimentation rate, it is crucial for the surplus ^{210}Pb (depicted in Figure 4.11) to diminish with depth, a trend that is not currently observed. Introducing additional data points between the existing ones is unlikely to yield a more pronounced declining pattern. The surplus ^{210}Pb

originates from the catchment, and it is plausible that significant variations in erosion, coupled with a potentially high sedimentation rate, hinder the discernment of a decline in 210Pb. Perhaps employing a longer core could offer valuable insights in this regard. Further data and discussions in chapter 5 (Discussion) are anticipated to provide additional insights and refine the sedimentation rate estimation for Griessee.

4.6 Mass Accumulation Rate

Having calculated an average sedimentation rate over depth for Triftsee, together with the results for dry bulk density allows us to come up with an estimation of mass accumulation rate (MAR) presented in Figure 4.12. The trend looks the same as for the results of dry bulk density alone because the sedimentation rate going in the calculation for the MAR was a constant over depth. In the Figure, one can see, that the mass accumulation rate decreases with depth. This could mean that there was higher input into the lake in the last years.

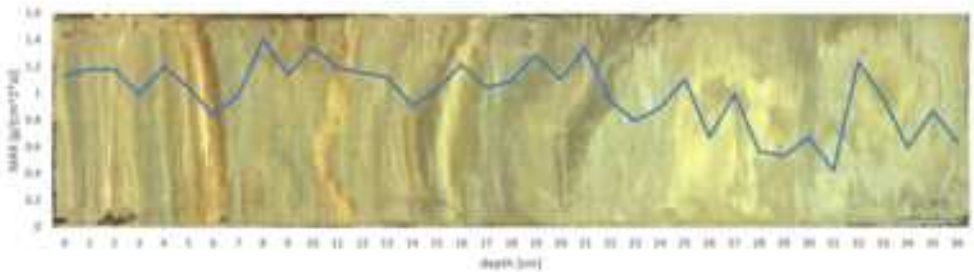

Figure 4.12: Mass accumulation rate for Triftsee, based on sedimentation rate of 0.8 cm per year and dry-bulk density values for every one-centimeter interval over depth.

For Griessee, a mass accumulation rate was not calculated due to limitations in the Gamma Analysis results, which prevented the derivation of a reliable estimate for a consistent sedimentation rate.

Chapter 5

Discussion

In this section, we aim to address the research questions outlined in Section 1.3 Research Questions based on the results obtained from various analyses presented in Section 4 Results.

5.1 Triftsee

To facilitate a comprehensive comparison of the results obtained from different analyses, the most significant and intriguing findings were collectively plotted against depth in Figure 5.1. Five specific depths were identified, marking points where trends began to shift.

At a depth of 2.2 cm, peaks in clay content coincide with variations in dry bulk density. This depth also reveals peaks in the ratios of Si/Ti, Al/Ti, and Zr/Rb as well as peaks in Rb and Sr.

Moving to 8.1 cm, a distinct peak in sand content aligns with a significant rise in dry bulk density. The coarser composition of sand particles compared to clay and silt offers a plausible explanation for the observed higher dry bulk density in this particular layer.

At a depth of 14.6 cm, there is a trough in sand content, mirrored by a decrease in dry bulk density, consistent with the earlier explanation. Simultaneously, this depth exhibits peaks in clay, Sr, Ti, Fe and the ratio of Zr/Rb.

Further down, at 20 cm a peak in the ratios Si/Ti, Si/Al, and Ba/Al coexists with troughs in Al, K, Fe, Ti, and dry bulk density. Additionally, a minor peak appears for sand and silt.

Finally, descending to 30 cm, a distinct peak in clay content is complemented by peaks in dry bulk density, Sr, and the ratio Zr/Rb.

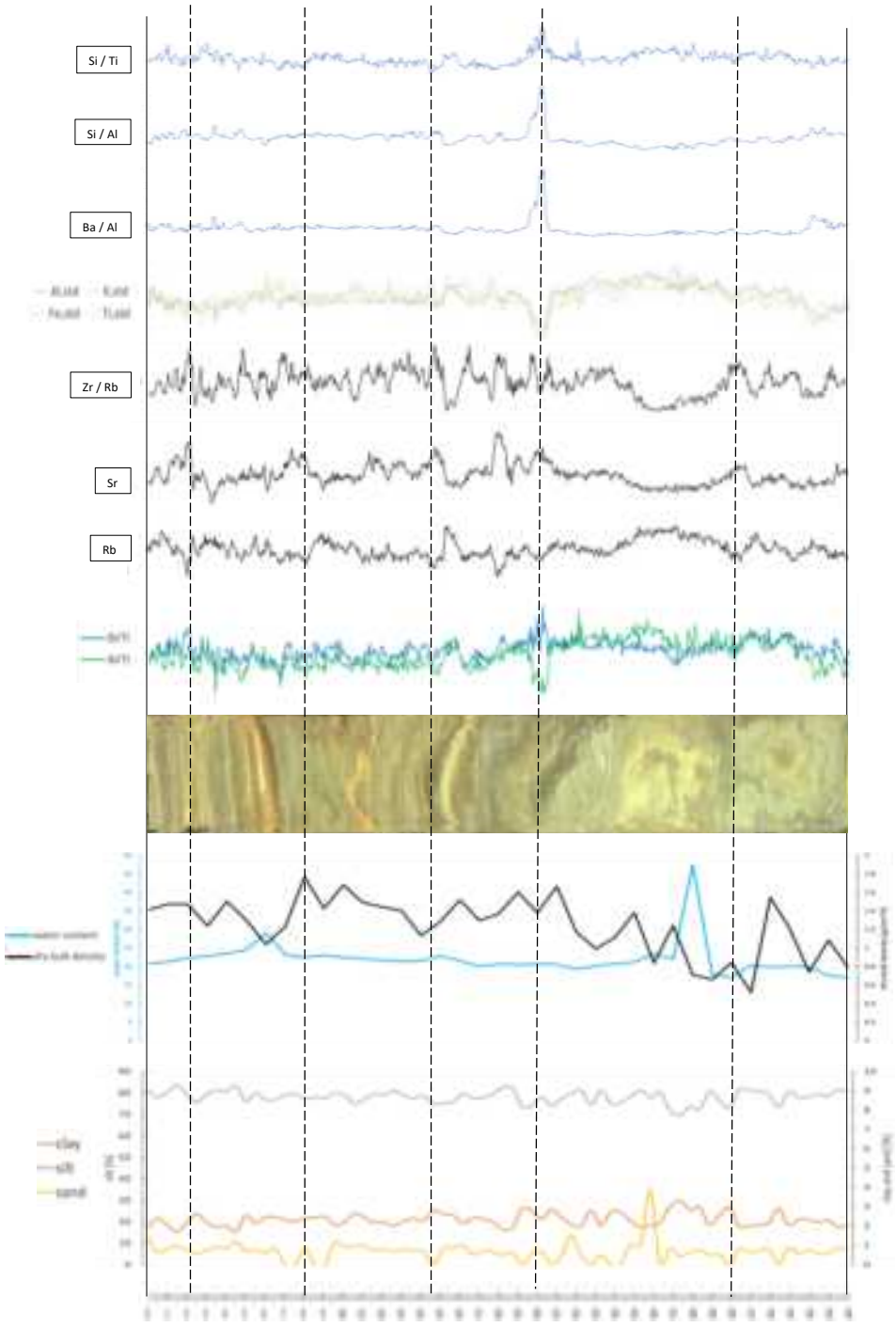

Figure 5.1: Results for elemental composition, dry bulk density, water content, and grain size analysis with depth, presented alongside the line scan.

As outlined in the introduction, winter peaks are expected to be characterized by higher clay concentrations. In the pursuit of detecting the winter clay layer, which might not be visible in the results obtained from particle size analyses due to sampling resolution limitations, the decision was made to include supplementary XRF-based indicators for tracking changes in grain size (Figure 5.2). This involved considering elements such as Sr and Rb, given that Sr and Rb are anticipated to correlate with the clay content in the sediment (Dypvik & Harris, 2001). Also the ratio of the Zr/Rb was plotted, because Zr/Rb ratios can be interpreted to indicate grain size variations (Fralick & Kronberg, 1997).

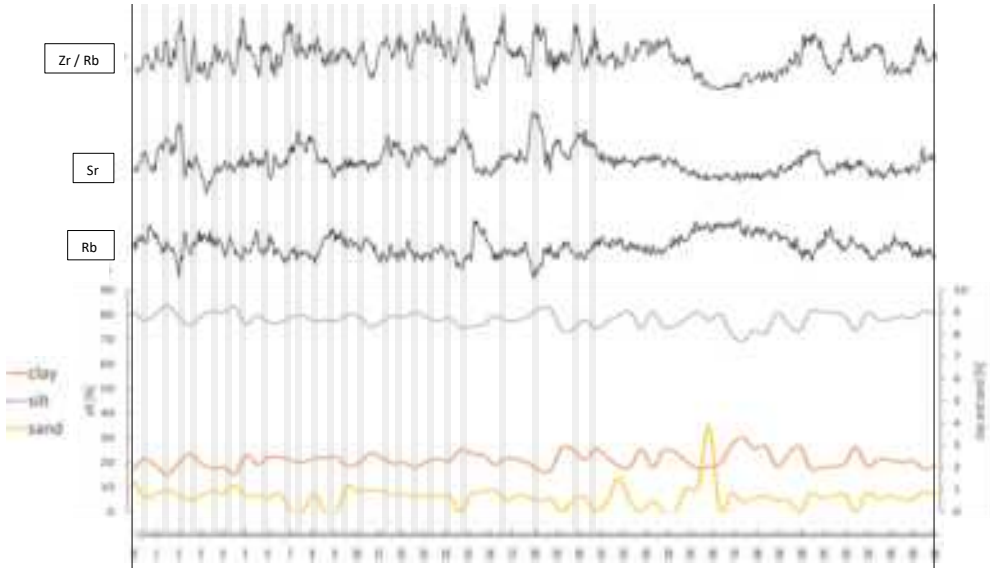

Figure 5.2: Sr, Rb and ratio of Zr/Rb plotted with depth next to results for grain size. Silt corresponds to the axis on the left, whereas content for clay and sand corresponds to the secondary axis on the right.

It is evident that the elemental proxies provide clearer insights in this context due to their higher resolution than grain size anaylsis. A total of 24 peaks were successfully identified in the lake sediment region, extending down to 21 cm, potentially corresponding to winter peaks and thereby representing 24 years. This estimation proves valuable, yielding a sedimentation rate of 0.88 cm/a, which aligns closely with the gamma analysis result of 0.91 cm/a.

To investigate, if the glacier retreat has an impact on the sedimentation in the lake, different results were plotted together with the glacier retreat for the last 45 years in Figure 5.3 (based on a sedimentation rate of 0.8 cm/a for the whole core based on gamma-spectroscopy).

For mean yearly temperature and the sum of annual precipitation, data was

collected from Meteo Schweiz for stations near Triftsee. Precipitation data was obtained from the Göscheneralp station (1745 m.a.s.l., LV95: 2681253, 1166804), while temperature data was gathered from the Meiringen station (589 m.a.s.l., LV95: 2655844, 1175930). Although having temperature data from Meiringen may not be optimal due to the altitude difference with Triftsee, which is nearly 1000 meters higher, it is still acceptable because we are analyzing trends and not absolute values in this graph.

The significance of annual temperature and rainfall data lies in unraveling factors influencing sediment discharge. Increased precipitation implies higher discharge, impacting erosion. Meanwhile, higher temperatures contribute to glacier melting and potential sediment transport.

In the graph, we attempted to identify points of interest, such as peaks, troughs, or the beginning and end of trends.

Examining the evolution of ice volume (1), Triftglacier has experienced a relatively slow and gradual melting over the past 30-40 years. This suggests that fluctuations in sediment input have been low during this period, supporting the simplification of calculating an average sedimentation rate for the entire core. However, since 2016, the melting appears to have increased, as indicated by steeper lines in volume (1) and area (2) evolution, marked by a vertical dashed line and higher negative values of glacier mass balance. Since 2020, the retreat seems to have intensified further, marked again by a straight vertical dashed line.

The mean annual temperature appears to have increased over the depicted period, while the sum of yearly precipitation varies with no clear trend. As discussed earlier, the mass accumulation rate (MAR) has increased over the whole core. But when looking only on the last 20 years since the lake came into existence (corresponding to roughly the upper 21 cm of the core according to the results of the gamma analysis with a sedimentation rate of 0.91 cm/a) it seems like MAR was higher between 21 and 6 cm depth. This coincides with the period when the glacier was in close proximity to the lake and undergoing backward melting. In the zone between 6 cm and the lake's surface, where the glacier experiences accelerated melting, the average MAR appears to be slightly lower than the interval between 21 and 6 cm. This trend is reflected in the thickness of sediment laminations, with the lower part exhibiting more substantial layers that gradually thin out in the upper part. Consequently, less sediment is deposited annually when the glacier is melting rapidly, compared to the earlier years.

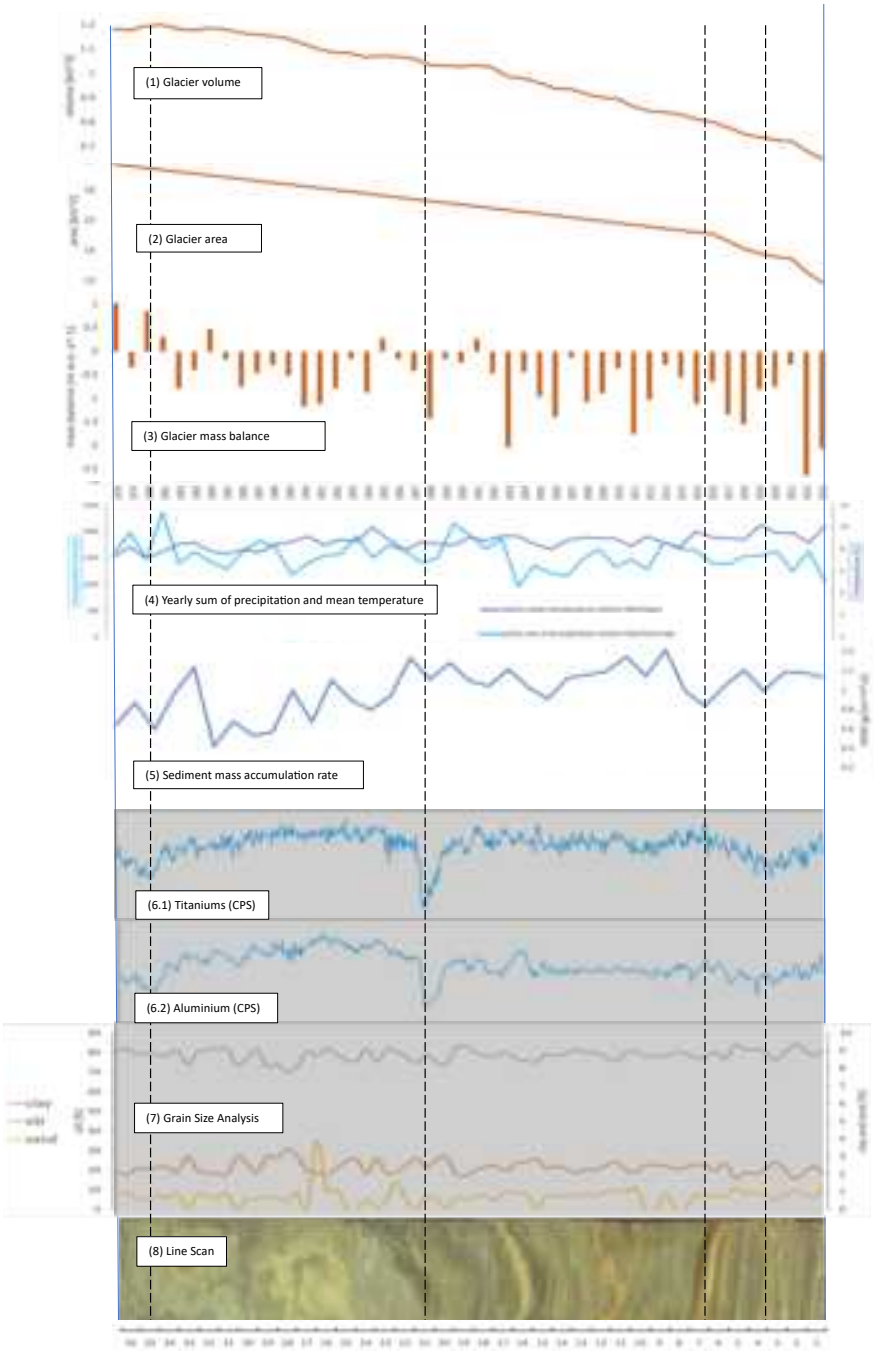

Figure 5.3: Results for glacier retreat in terms of volume (1), area (2), and mass balance (3) together with the yearly sum of precipitation for the station of Göscheneralp and mean annual temperature for the station of Meiringen. Results for mass accumulation rate (MAR), Titanium and Aluminium CPS values, grain size analysis, and line scan. Results cover the period from 1978 to 2023, as indicated by gamma analysis suggesting an approximate age of 45 years for the core.

The specific reasons for this phenomenon are not entirely clear. It could be attributed to the upper part of the glacier melting more rapidly, resulting in reduced mobilization of sediment from below. Another possibility is that the glacier has ceased to recede, no longer grounding the bedrock. Additionally, sediment might be deposited in the catchment rather than in the lake when the glacier is situated farther away.

In the year around 1980 (marked by a straight vertical dashed line), a positive mass balance, a slight increase in glacier volume, a MAR trough, and troughs in mean temperature, sum of precipitation, Titanium (Ti), and Aluminum (Al) were identified. This suggests that in that year, there was less precipitation (lower erosion) and lower temperatures (reduced glacier melting), resulting in a positive glacier mass balance and reduced sediment input, as indicated by Ti and Al signals.

Around 1998, strong troughs in Al and Ti, along with a significant negative mass balance of the glacier, precipitation trough, and peaks in silt and sand were observed. This contradicts the earlier hypothesis, as troughs in Al and Ti would indicate lower input to the lake, but a negative glacier mass balance would suggest higher input for that year. A reason for these strong peaks could also be, that it was in that period when Triftsee came into existence.

5.2 Griessee

To compare the results for the different analyses, the most important and interesting ones were plotted together with depth in Figure 5.4, as was done for Triftsee. It must be noted that in 2015, Griessee was nearly completely drained, and the discharge level for water in the dam structure was increased. This factor should be taken into account in the analysis of the results.

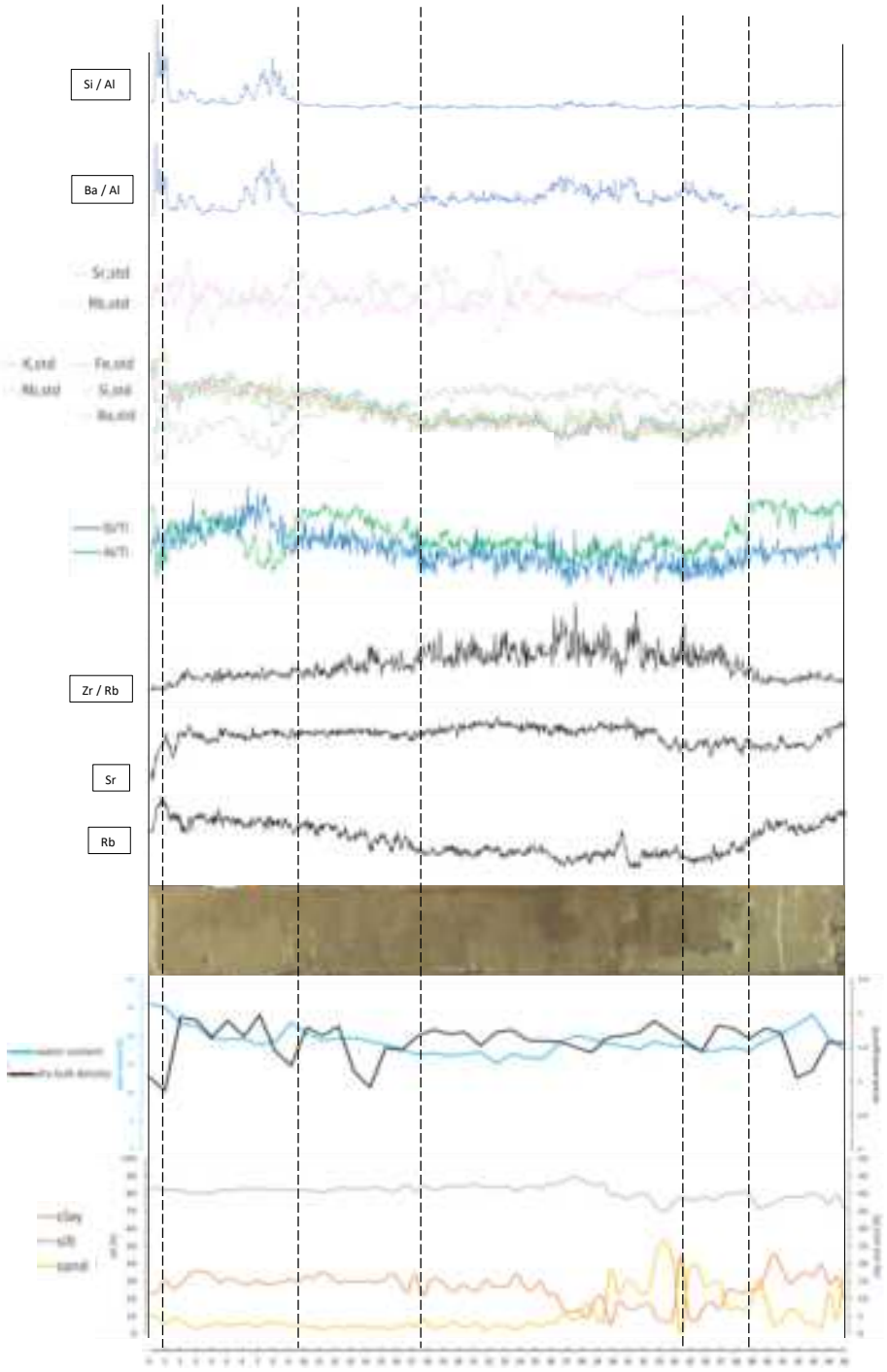

Figure 5.4: Results for elemental composition, dry-bulk density, water content, and grain size analysis with depth next to the line scan.

Five interesting depths were identified, marking spots where trends started to change.

At a depth of 1 cm, peaks are observed for ratios of Si/Al and Ba/Al, along with peaks for Rb and Sr. Also dry bulk density exhibits a peak, and there is an additional peak for clay, while the sand content decreases.

Moving to a depth of 9.7 cm, a concluding trend is noted with peaks in the ratios of Si/Al and Ba/Al. A peak for Sr is observed, signifying the end of peaks in the ratios of Si/Ti and Al/Ti.

At 17.7 cm depth, there is a peak in sand content, a decrease in clay content, and an additional peak for silt. Dry bulk density is observed to be increasing.

Reaching a depth of 34.5 cm, there is a transition from high clay content to high sand content. A small peak for Ba/Al is also observed.

At 38.9 cm depth, both sand and clay contents start to increase, resulting in a decrease in silt. A valley is observed in dry bulk density, while Rb is increasing. Additionally, there is an increase in the ratios of Si/Ti and Al/Ti.

As described in the result section for Griessee, there are two prominent peaks at depths of 1-2 and 7-9 centimeters for the Si/Al and Ba/Al ratios. This could indicate an increase in primary production at these depths, as Si and Ba are indicative thereof (especially Si for diatoms) (Holder et al., 2020).

Since the Gamma results did not yield a robust sedimentation rate, alternative approaches were explored to estimate sedimentation rates.

Initially, for Griessee, attempts were made to identify winter peaks by plotting clay content against Sr and Rb abundance over depth (Figure 5.5). A total of 25 locations with peaks in clay content corresponding to peaks in Sr and Rb abundance were identified. This suggests that the sediment core from Griessee may contain sediment spanning the last 25 years, resulting in a potential mean sedimentation rate of 1.8 cm/year. It is important to note that the grain size analysis resolution was limited to 0.5 cm intervals, potentially impacting the accurate representation of clay peaks as discussed before for Triftsee.

Similar to Triftsee, this hypothesis was further examined by plotting the Zr/Rb ratio against grain size distribution over depth (Figure **??**), as Zr/Rb ratios can indicate variations in grain size (Fralick & Kronberg, 1997). 27 regions were identified with peaks in the Zr/Rb ratio aligned with slight changes in grain size distribution, confirming the assumption that the sediment core from Triftsee corresponds to approximately 25 years, with an estimated sedimentation rate of around 1.8 cm/a.

An additional approach to estimate sedimentation rates in Griessee involved calculating the reservoir volume using bathymetric measurements. Con-

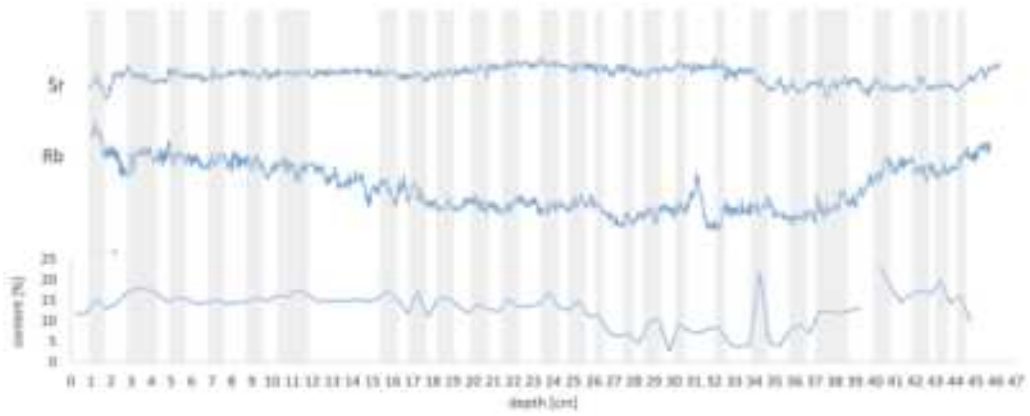

Figure 5.5: Strontium and Rubidium next to clay content with depth for Griessee.

ducted four times between 2011 and 2021, these measurements allowed for assessing volume changes at one-meter intervals. Extrapolating these volumes over time, considering the lake's surface area of 59.4 hectares, resulted in an average sedimentation rate of 7 cm/a (Figure 5.7). This suggests that the 45-centimeter extracted core corresponds to the last 6-7 years, given the sedimentation rate of around 7 cm/a.

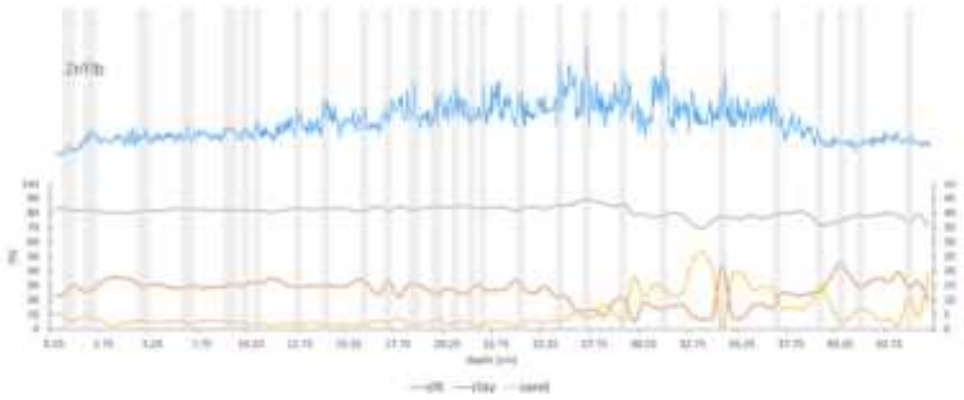

Figure 5.6: Ratio of Zr to Rb next to grain size distribution for Griessee. Content for silt corresponds to the axis on the left, whereas content for clay and sand corresponds to the secondary axis on the right.

Previous work by Ehrbar et al. (2017) stated that 618,240 m^3 of sediment were deposited in Griessee between 1976 and 2011. Calculating the sedimentation rate based on this number and a lake surface area of 59.4 ha resulted in a sedimentation rate of 3 cm per year during that period. Compared to the sedimentation rate based on the bathymetry measurements from 2011-

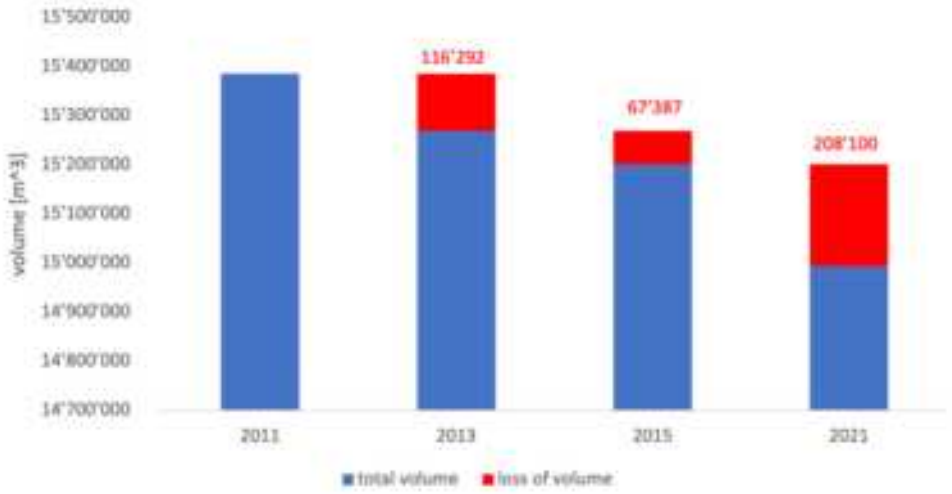

Figure 5.7: Total volume and loss of volume of Griessee for the years 2011, 2013, 2015, and 2021. Bathymetry measurements conducted by CONSULTEST SA.

2021, this suggests an increase in sedimentation rate, aligning with the fast decrease of the glacier due to global warming, as reported by (Ehrbar et al., 2017).

This results in five different hypotheses for the sedimentation rate of Griessee (Table 5.1):

Table 5.1: Hypotheses for sedimentation rate of Griessee.

Estimation	Reasoning
0.53 cm/a	Unsupported ^{210}Pb concentrations for whole core
1.8 cm/a	Clay-, Strontium-, and Rubidium-peaks
1.94 cm/a	^{210}Pb concentrations for [0-30cm] depth
3 cm/a	Calculations based on sedimentation volume for 1976 - 2011 (Ehrbar et al., 2017)
7 cm/a	Calculations based on bathymetry measurements of CONSULTEST SA (2011-2021)

Excluding the lowest and highest estimations, the sedimentation rate is likely to fall within the range of 2-3 cm/a.

5.3 Comparison

In this section, we explore the differences in sedimentation between Triftsee, a natural and still untouched glacier lake, and Griessee, a dammed glacier lake, based on our obtained results.

It's crucial to note that our study is limited by having only one lake for each type (natural vs. dammed), impacting the representativeness of the results. Furthermore, as discussed later, the observed differences are most likely not due to the damming of the lake but more a result of distinct geological contexts and varied catchment characteristics, including precipitation, temperature, rock types, and slope gradients. The influence of the dam would be more on trapping the sediments after entering the lake and not leaving the lake again with the outflow.

As demonstrated earlier, there is a discernible difference in sedimentation rates between the two lakes. The rapid glacier retreat observed in Griessee (for almost a hundred years, Gries has experienced predominantly negative mass balance years, whereas for Trift, a significant decrease has only become apparent in the last few decades) illustrated in Figures 2.11 suggests higher absolute negative mass balance values and a consistently negative mass balance over an extended period. This implies increased sediment input into Griessee, likely associated with the glacier's behavior rather than the damming of the lake.

Examining grain size reveals that Griessee has a higher sand content than Triftsee. This difference is not attributed to the natural or dammed state of the lake but is influenced by the rock types present in their respective catchments. The size, composition, and density of sediments influence settling rates, with fine-grained sediments potentially staying suspended in water for longer periods, affecting sedimentation rates. This could mean that the sedimentation rate for Triftsee could be smaller because of the higher clay content of the sediment in Triftsee compared to Griessee.

Despite Triftsee having a larger catchment area, smaller lake size, and steeper slopes (mean slope of the catchment = 25%), it experiences less sedimentation compared to Griessee. On the other hand, Griessee, with a smaller catchment area and milder slopes (mean slope of the catchment = 17%), exhibits a higher relative sedimentation rate and absolute sedimentation volume.

The size, shape, and depth of the lake can also influence sedimentation rates. In this case, the bathymetries have similar shapes with maximum depths occurring at around 2/3 of the lake length (starting from the delta in the direction of the outlet) and roughly equivalent maximum depths. Just the total volume and lake surface area differ.

Vegetation cover can also play a role, with thriving plants potentially trap-

ping sediments entering the lake. However, this is not a strong factor for both lakes, as there is minimal vegetation cover in their catchment areas (3% for Triftsee and 0% for Griessee).

Visually, sediment in Triftsee displays more natural lamination than in Griessee, likely due to a less disturbed environment with minimal human impact. Triftsee also exhibits clearer peaks in grain size analysis, supporting the thesis of an undisturbed environment without rapid lake level changes, water releases, changes in shoreline structure, or complete reservoir drainage, as occurred in Griessee in 2015 (all factors because of hydropower production).

Chapter 6

Conclusion

6.1 Summary

In this semester project, the aim was to investigate the sedimentation rates of a natural glacier lake and a dammed glacier lake, attempting to calculate the sedimentation rate for each. Additionally, a comparison of sedimentation between the two lakes was conducted. Two study areas were selected: the natural Triftsee in the canton of Bern and the dammed Griessee in the canton of Valais. During fieldwork, sediment cores were extracted from both lakes. These cores were then analyzed using various laboratory methods.

A high-resolution image of each core was obtained through a line scan. Subsequently, XRF analysis was performed to determine the elemental composition at different depths within the core. Measurements of dry-bulk density and water content were taken, and the mass accumulation rate was calculated. Finally, gamma spectroscopy was employed for dating purposes.

The results from the line scan revealed laminations in the Triftsee core, while the Griessee core did not exhibit such features. Elemental analysis provided insights into periods of increased terrestrial input, shedding light on environmental changes. Water content and dry bulk density did not display clear trends. Grain size analysis gave an interesting insight into the fractions of clay, silt, and sand at different depths, and peaks of different fractions could be linked to trends in elemental composition. Gamma spectroscopy allowed the calculation of a sedimentation rate of 0.91 cm/year up to a depth of 21 cm for the Triftsee. However, the gamma analysis for the Griessee did not yield clear results. Various hypotheses suggest that the sedimentation rate for the Griessee may be higher, approximately 2-3 cm/year.

The disparity in sedimentation rates is likely less related to the fact that Griessee is dammed and more associated with differences in catchment characteristics between the two lakes. However, the dam exerts an influence on

the sediment dynamics in the rivers downstream of the lake.

6.2 Outlook

In the pursuit of refining sedimentation analysis for glacier lakes, several key avenues for future research emerge, providing a comprehensive outlook for enhanced understanding.

Firstly, addressing the current limitation of relying on a single core per lake is paramount. To achieve a more representative assessment, more sedimentation cores need to be retrieved. This can be accomplished by revisiting the lakes in winter when the surface is frozen, allowing heavier equipment to penetrate the compacted sediment. Multiple cores per lake should be extracted to capture the heterogeneity.

Enhancing the spatial resolution of sedimentation rate analysis involves a more thorough consideration of factors such as distance to the outlet, delta, shoreline, as well as the depth and slope of the lake bed. By integrating these parameters, a more nuanced understanding of sedimentation patterns can be achieved.

Temporal resolution is another area that can be improved. Rather than calculating a constant sediment rate for the entire core, future analyses should explore sediment rates for individual years or specific time frames. This temporal granularity will provide a more accurate depiction of sedimentation trends over time.

Conducting independent bathymetry measurements is recommended to augment existing datasets. By employing bathymetric assessments, essential information about lake depths and terrain slopes can be determined, facilitating a more accurate calculation of sedimentation rates for the entire lake and enabling the development of sediment budgets.

Moreover, the relationship between sedimentation rates and catchment erosion rates is a crucial aspect that demands exploration. Understanding this connection will contribute to a more holistic perspective on the interplay between sedimentation within the lake and external factors influencing catchment erosion.

Furthermore, the results for the sedimentation rate should be analyzed together with the ≪Spezialbefliegungen≫ datasets, especially with the results of other working packages of the TapRep project. This offers a unique opportunity to examine how changes in terrain within the catchment relate to sedimentation rates. This interdisciplinary approach can uncover valuable insights into the dynamic interactions between topographical alterations and sedimentation processes.

To refine dating methodologies, a higher resolution of data points for the unsupported ^{210}Pb concentrations is recommended. This will address temporal uncertainties and provide a more accurate timeline for sedimentation processes.

Looking ahead to future reservoir dam projects in glacier lakes, sedimentation must be a central consideration in planning. The direct influence on reservoir capacity underscores its significance in determining the profitability and sustainability of hydropower ventures. Recognizing the unique characteristics of each lake and its catchment is crucial for tailored and effective solutions. Consideration must also be given to the fact that a dam significantly impacts the sediment dynamics downstream of the lake and the ecology of the surrounding habitats.

Chapter 7

Acknowledgements

I would like to express my sincere gratitude to Ronald Lloren, my mentor, for his invaluable guidance throughout this project, particularly for his assistance in the laboratory. I extend my thanks to Nathalie Dubois and Daniel Farinotti for supervising my work and providing me with the opportunity to delve into the interesting topics of glaciers and sedimentation.

Special appreciation goes to the entire team at Eawag for their support during the fieldwork, and to the dedicated technicians in the sedimentology group at Eawag for their assistance with the analysis in the laboratory.

I also want to extend my gratitude to VAW Zurich for generously providing data on the glacier retreat of Gries and Trift.

Appendix A

Appendix

Figure A.1: Map of extent of Triftglacier in different time periods. (Swisstopo, 2023).

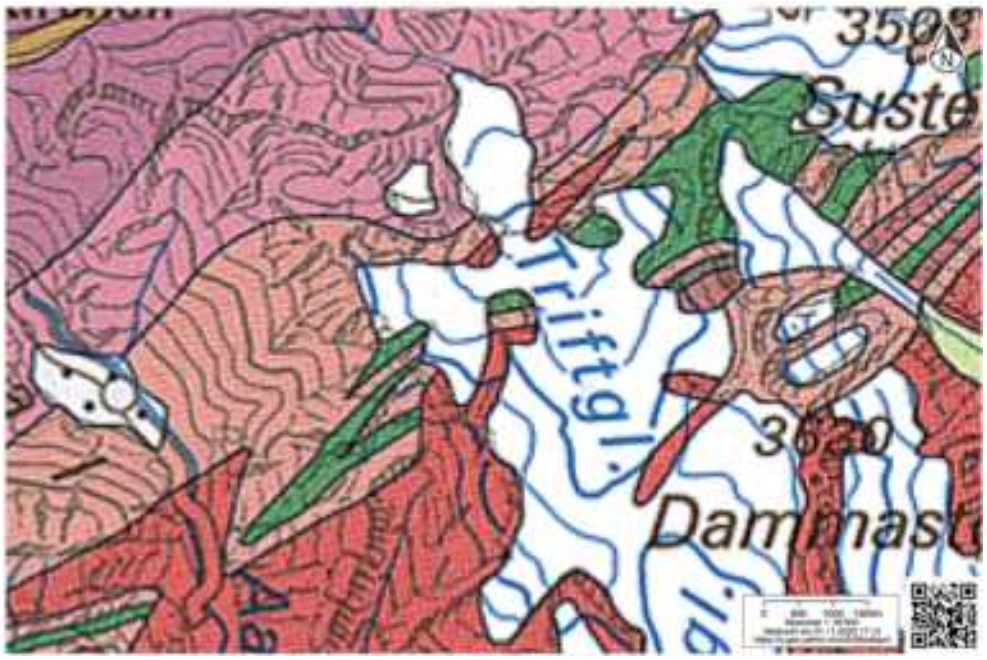

Figure A.2: Map of geology of catchment of Trift (Swisstopo, 2023). Marked in yellow is the part with amphibolites. Legend can be found under map.geo.admin.ch.

Figure A.3: Areal view of the first signs of a glacial lake in the catchment of Triftsee at the beginning of the millennium (Swisstopo, 2023)

.

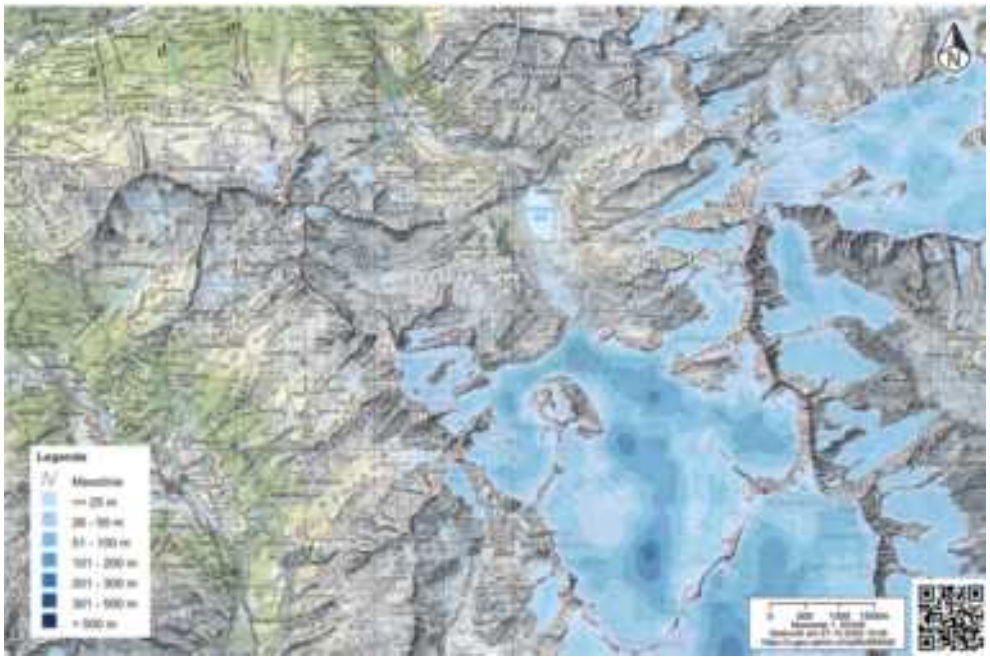

Figure A.4: Map of thickness Trift glacier. (Swisstopo, 2023)

Figure A.5: Map of the thickness of Gries glacier. (Swisstopo, 2023)

Figure A.6: Map of glacier extent of Gries glacier in the year 1958 (Swisstopo, 2023).

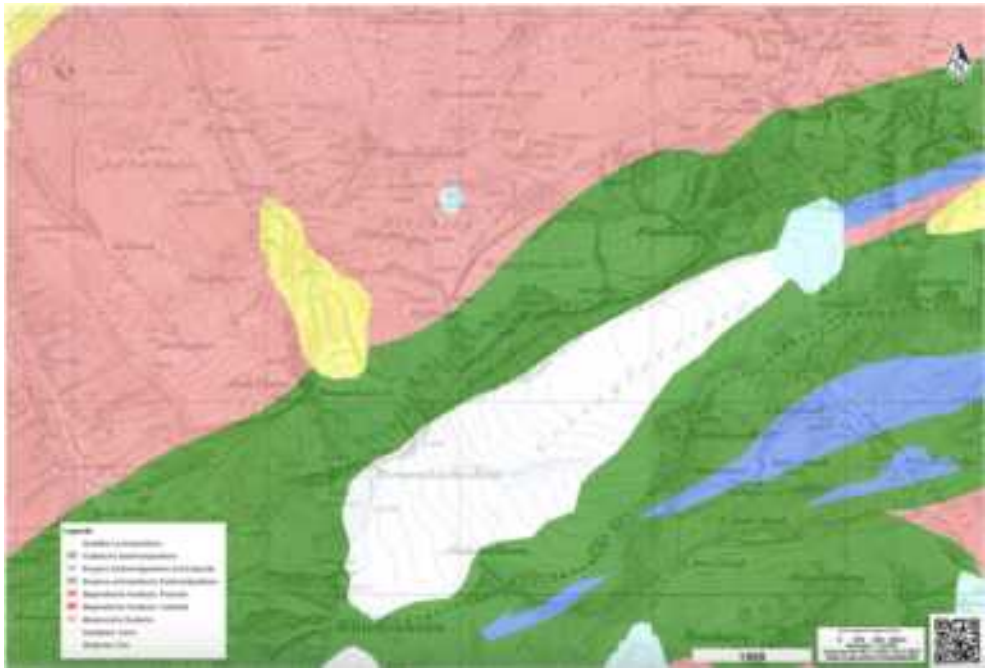

Figure A.7: Map of formation of rocks for the catchment of Griessee (Swisstopo, 2023).

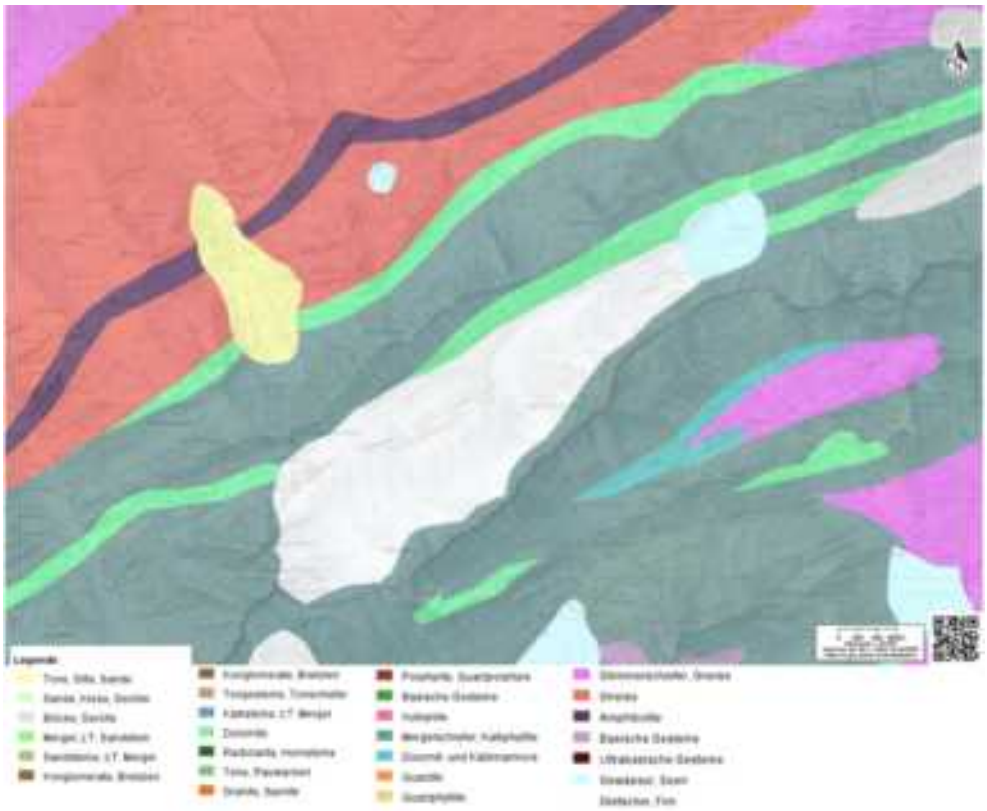

Figure A.8: Map of lithology for the catchment of Griessee (Swisstopo, 2023).

Bibliography

Aber, J. (2008). Land-system approach applied to glacial geomorphology. *Boreas*, *33*, 95–96. https://doi.org/10.1111/j.1502-3885.2004.tb00999.x

Arnaud, F., Poulenard, J., Giguet-Covex, C., Wilhelm, B., Revillon, S., Jean-Philippe, J., Revel, M., Enters, D., Bajard, M., Fouinat, L., Doyen, E., Simonneau, a., Pignol, C., CHAPRON, E., Vannière, B., & Sabatier, P. (2016). Erosion under climate and human pressures: An alpine lake sediment perspective. *Quaternary Science Reviews*, *152*. https://doi.org/10.1016/j.quascirev.2016.09.018

Ballantyne, C. (2002). Paraglacial geomorphology. *Quaternary Science Reviews - QUATERNARY SCI REV*, *21*, 1935–2017. https://doi.org/10.1016/S0277-3791(02)00005-7

Baumer, A. (2015). *Gries-staumauer* (tech. rep.). Ofima SA.

Boyle, J. (2000). Rapid elemental analysis of sediment samples by isotope source xrf. *Journal of Paleolimnology*, *23*. https://doi.org/10.1023/A:1008053503694

Callieri, C. (1997). Sedimentation and aggregate dynamics in lake maggiore, a large, deep lake in northern italy. *Memorie dell' Istituto Italiano di Idrobiologia*, *56*.

Chen, J., Wilson, C., & Tapley, B. (2013). Contribution of ice sheet and mountain glacier melt to recent sea level rise. *Nature Geoscience*, *6*, 549–552. https://doi.org/10.1038/ngeo1829

Christoudias, T., & Lelieveld, J. (2013). Modelling the global atmospheric transport and deposition of radionuclides from the fukushima daiichi nuclear accident. *Atmospheric Chemistry and Physics*, *13*. https://doi.org/10.5194/acp-13-1425-2013

Cook, S., & Swift, D. (2012). Subglacial basins: Their origin and importance in glacial systems and landscapes. *Earth-Science Reviews*, *115*, 332–372. https://doi.org/10.1016/j.earscirev.2012.09.009

Dalban Canassy, P., Bauder, A., Dost, M., Fäh, R., Funk, M., Margreth, S., Müller, B., & Sugiyama, S. (2011). Hazard assessment investigations due to recent changes in triftgletscher, bernese alps, switzerland. *Natural Hazards and Earth System Sciences - NAT HAZARDS EARTH SYST SCI*, *11*, 2149–2162. https://doi.org/10.5194/nhess-11-2149-2011

Delaney, I., Bauder, A., Huss, M., & Weidmann, Y. (2017). Proglacial erosion rates and processes in a glacierized catchment in the swiss alps. *Earth Surface Processes and Landforms*, *43*. https://doi.org/10.1002/esp.4239

Dypvik, H., & Harris, N. B. (2001). Geochemical facies analysis of fine-grained siliciclastics using th/u, zr/rb and (zr+rb)/sr ratios. *Chemical Geology*, *181*(1-4), 131–146.

Ehrbar, D., Schmocker, L., Doering, M., Cortesi, M., Bourban, G., Boes, R., & Vetsch, D. (2018). Continuous seasonal and large-scale periglacial reservoir sedimentation. *Sustainability*, *10*, 3265. https://doi.org/10.3390/su10093265

Ehrbar, D., Schmocker, L., Vetsch, D., Boes, R., & Doering, M. (2017). Measuring suspended sediments in periglacial reservoirs using water samples, lisst and adcp. *International Journal of River Basin Management*, *15*, 1–18. https://doi.org/10.1080/15715124.2017.1327866

Fralick, P., & Kronberg, B. (1997). Geochemical discrimination of clastic sedimentary rock sources. *Sedimentary Geology*, *113*, 111–124. https://doi.org/10.1016/S0037-0738(97)00049-3

Gisler, C., Labhart, T., Spillmann, P., Herwegh, M., Della Valle, G., TrüsseL, M., & Wiederkehr, M. (2020). 1210 innertkirchen. *Geol. Atlas Schweiz 1:25000*.

Grischott, R., Anselmetti, F., & Funk, M. (2010). Seismic survey lake trift, tech. rep. *Mitteilungen 224, Versuchsanstalt für Wasserbau, Hydrologie und Glaziologie (VAW)*.

HADES. (2023). Hydrologischer atlas der schweiz.

Haeberli, W., Hoelzle, M., Paul, F., & Zemp, M. (2007). Integrated monitoring of mountain glaciers as key indicators of global climate change: The european alps. *Annals of Glaciology*, *46*. https://doi.org/10.3189/172756407782871512

Hock, R., & Huss, M. (2021). Glaciers and climate change. https://doi.org/10.1016/B978-0-12-821575-3.00009-8

Holder, L., Duffy, M., Opdyke, B., Leventer, A., Post, A., O'Brien, P., & Armand, L. (2020). Controls since the mid-pleistocene transition on sedimentation and primary productivity downslope of totten glacier, east antarctica. *Paleoceanography and Paleoclimatology*, *35*. https://doi.org/10.1029/2020PA003981

Huss, M. (2011). Present and future cotribution of glacier storage change to runoff from macroscale drainage basins in europe. *Water Resources Research*, *47*, W07511. https://doi.org/10.1029/2007WR010299

Huss, M., Jouvet, G., Farinotti, D., & Bauder, A. (2010). Future high-mountain hydrology: A new parameterization of glacier retreat. *Hydrology and Earth System Sciences*, *14*, 815–829. https://doi.org/10.5194/hessd-7-345-2010

Kumar, U., Navada, S., Rao, S., Nachiappan, R., Kumar, B., Krishnamoorthy, T., Jha, S., & Shukla, V. (1999). Determination of recent sedimentation rates and pattern in lake naini, india by 210pb and 137cs dating techniques. *Applied Radiation and Isotopes - APPL RADIAT ISOTOPES*, *51*, 97–105. https://doi.org/10.1016/S0969-8043(98)00148-1

Leonard, E. M. (1986). Varve studies at hector lake, alberta, canada, and the relationship between glacial activity and sedimentation. *Quaternary Research*, *25*(2), 199–214. https://doi.org/10.1016/0033-5894(86)90057-8

Mabit, L., Moncef, B., & Walling, D. (2008). Comparative advantages and limitations of fallout radionuclides (137cs, 210pb and 7be) to assess soil erosion and sedimentation. *Journal of environmental radioactivity*, *99*, 1799–1807.

Matisoff, G., & Whiting, P. (2011). Measuring soil erosion rates using natural (7be, 210pb) and anthropogenic (137cs, 239,240pu) radionuclides. https://doi.org/10.1007/978-3-642-10637-8_25

Mauchle, F. (2010). *The modern sediments of lake oeschinen (swiss alps) as an archive for climatic and meteorological events*.

Menzies, J., & Ross, M. (2020). Glacial processes and landforms—transport and deposition. https://doi.org/10.1016/B978-0-12-818234-5.00027-4

Mölg, N., Huggel, C., Herold, T., Storck, F., Allen, S., Haeberli, W., Schaub, Y., & Odermatt, D. (2021). Inventory and evolution of glacial lakes since the little ice age: Lessons from the case of switzerland. *Earth Surface Processes and Landforms*, *46*. https://doi.org/10.1002/esp.5193

Myrstener, E., Ninnes, S., Meyer-Jacob, C., Mighall, T., & Bindler, R. (2021). Long-term development and trajectories of inferred lake-water organic carbon and ph in naturally acidic boreal lakes. *Limnology and Oceanography*, *66*. https://doi.org/10.1002/lno.11761

Putyrskaya, V., Klemt, E., Röllin, S., Astner, M., & Sahli, H. (2015). Dating of sediments from four swiss prealpine lakes with 210pb determined by gamma-spectrometry: Progress and problems. *Journal of Environmental Radioactivity*, *145*, 78–94. https://doi.org/10.1016/j.jenvrad.2015.03.028

Salim, E. (2022). Glacier tourism and climate change in switzerland. https://doi.org/10.4337/9781839100185.00010

Schleiss, A., Franca, M., Juez, C., & De Cesare, G. (2016). Reservoir sedimentation. *Journal of Hydraulic Research*, *54*, 1–20. https://doi.org/10.1080/00221686.2016.1225320

Steffen, T., Huss, M., Estermann, R., Hodel, E., & Farinotti, D. (2022). Volume, evolution, and sedimentation of future glacier lakes in switzerland over the 21st century. *Earth Surface Dynamics*, *10*, 723–741. https://doi.org/10.5194/esurf-10-723-2022

Steinemann, O., Ivy-Ochs, S., Hippe, K., Christl, M., Haghipour, N., & Synal, H.-A. (2021). Glacial erosion by the trift glacier (switzerland): Deciphering the development of riegels, rock basins and gorges. *Geomorphology*, *375*, 107533. https://doi.org/10.1016/j.geomorph.2020.107533

Swift, D., Tallentire, G., Farinotti, D., Cook, S., Higson, W., & Bryant, R. (2021). The hydrology of glacier-bed overdeepenings: Sediment transport mechanics, drainage system morphology, and geomorphological implications. *Earth Surface Processes and Landforms*, *46*. https://doi.org/10.1002/esp.5173

Swisstopo. (2023). Maps of switzerland.

Vuille, M., Francou, B., Wagnon, P., Juen, I., Kaser, G., Mark, B., & Bradley, R. (2008). Climate change and tropical andean glaciers: Past, present and future. *Earth-Science Reviews*, *89*, 79–96. https://doi.org/10.1016/j.earscirev.2008.04.002

Weltje, G., & Tjallingii, R. (2008). Calibration of xrf core scanners for quantitative geochemical logging of sediment cores: Theory and application. *Earth and Planetary Science Letters*, *274*, 423–438. https://doi.org/10.1016/j.epsl.2008.07.054

Wisser, D., Frolking, S., Hagen, S., & Bierkens, M. (2013). Beyond peak reservoir storage? a global estimate of declining water storage capacity in large reservoirs. *Water Resources Research*, *49*, 5732–5739. https://doi.org/10.1002/wrcr.20452

Zolitschka, B., Francus, P., Ojala, A., & Schimmelmann, A. (2015). Varves in lake sediments – a review. *Quaternary Science Reviews*, *117*, 1–41. https://doi.org/10.1016/j.quascirev.2015.03.019

Eidgenössische Technische Hochschule Zürich
Swiss Federal Institute of Technology Zurich

Declaration of originality

The signed declaration of originality is a component of every semester paper, Bachelor's thesis, Master's thesis and any other degree paper undertaken during the course of studies, including the respective electronic versions.

Lecturers may also require a declaration of originality for other written papers compiled for their courses.

I hereby confirm that I am the sole author of the written work here enclosed and that I have compiled it in my own words. Parts excepted are corrections of form and content by the supervisor.

Title of work (in block letters):

Comparing the sediment dynamics of a natural and a dammed glacier lake

Authored by (in block letters):

For papers written by groups the names of all authors are required.

Name(s):	**First name(s):**
Odermatt	Georg

With my signature I confirm that

- I have committed none of the forms of plagiarism described in the 'Citation etiquette' information sheet.
- I have documented all methods, data and processes truthfully.
- I have not manipulated any data.
- I have mentioned all persons who were significant facilitators of the work.

I am aware that the work may be screened electronically for plagiarism.

Place, date	**Signature(s)**
Zurich, 22.12.2023	

For papers written by groups the names of all authors are required. Their signatures collectively guarantee the entire content of the written paper.